DESIGN OPTIMIZATION FOR MINIMIZING THE PRODUCTION COST OF LITHIUM ION BATTERIES IN ELECTRIFIED VEHICLES

by
SAHAR DADASHI FARKHANDI

Submitted to the Graduate School of Engineering and Natural Sciences
in partial fulfilment of
the requirements for the degree of
Master of Science

Sabancı University
July 2023

DESIGN OPTIMIZATION FOR MINIMIZING THE PRODUCTION COST OF LITHIUM ION BATTERIES IN ELECTRIFIED VEHICLES

Approved by:

Date of Approval:.....

Abstract

DESIGN OPTIMIZATION FOR MINIMIZING THE PRODUCTION COST OF LITHIUM ION BATTERIES IN ELECTRIFIED VEHICLES

Sahar Dadashi Farkhandi

Energy Technologies and Management, Master's Thesis, July 2023

Thesis Supervisor: Assist. Prof. Dr. Tuğçe Yüksel

Keywords: Lithium-ion batteries, Battery design optimization, Battery production cost, Electric vehicle batteries

It has been recognized that the high cost of lithium-ion batteries (LIB) for electrified vehicles (EV) is one of the major obstacles to the commercialization of them. There is an ongoing effort to reduce the cost of LIBs both at the cell and the pack levels. This requires accurate cost and performance models of LIBs.

Our goal in this study was to obtain the best design for specific performance and design requirements in order to minimize production costs. We develop our battery model based on the Argonne National Laboratory's battery performance and cost model (BatPaC 5.0). A process-based cost model was utilized to model the production cost of the LIB by defining all the production steps and their process assumptions for a battery manufacturing plant. An optimization problem is defined by identifying decision variables from design parameters that have remarkable effects on the battery cost and performance. Cost optimization was done for four different vehicle types and four cathode chemistries. It is concluded that batteries made of NMC811 cathodes have the lowest costs among the four chemistries. Additionally, high-range battery electric vehicles (BEV) have the lowest specific costs in $ per kg. Several case studies were conducted to investigate the effects of changes in the production volume or battery performance requirements on the optimized design and production costs. As a result of these studies, we concluded that increasing the production volume will decrease the battery pack production cost. Increasing cathode thickness is an effective measure for decreasing costs. 30 and 15-minute fast charging will limit the cathode thickness.

ÖZET

ELEKTRİKLİ ARAÇLARDA LİTYUM İYON BATARYALAR ÜRETİM MALİYETİNİN EN AZA İNDİRİLMESİ İÇİN TASARIM ENİYİLEMESİ

SAHAR DADASHI FARKHANDI

Enerji Teknolojileri ve Yönetimi, Yüksek Lisans Tezi, Temmuz 2023

Tez Danışmanı: Assist. Prof. Dr. Tuğçe Yüksel

Anahtar Kelimeler: lityum-iyon bateryalar, Batarya tasarım eniyilemesi, Batarya üretim maliyeti, Elektrikli araçlar bataryaları

Elektrikli araçlar için lityum-iyon bataryaların (LİB) yüksek maliyetinin, elektrikli araçların ticarileştirilmesinin önündeki en büyük engellerden biri olduğu kabul edilmiştir. Bu nedenle LİBlerin maliyetlerini düşürmek için birçok çalışma yapılmaktadır. Bu çalışmalarda doğruluğu yüksek batarya performans ve maliyet modelleri önem taşımaktadır.

Bu çalışmanın amacı, belirli performans ve tasarım gereksinimleri altında üretim maliyetlerini en aza indirecek en iyi tasarımı elde etmektir. Bu amaçla Argonne Ulusal Laboratuvarı'nın batarya performansı ve maliyet modeline (BatPaC 5.0) dayalı bir batarya modeli geliştirilmiştir. Bir pil üretim tesisi için tüm üretim adımları ve bunların süreç varsayımları tanımlanarak LİB'nin üretim maliyetini modellemek için süreç tabanlı bir maliyet modeli kullanılmıştır. Pil maliyeti ve performansı üzerinde dikkate değer etkileri olan tasarım parametrelerinden karar değişkenlerini belirlenerek bir optimizasyon problemi tanımlanmıştır. Dört farklı araç tipi ve dört farklı katot kimyası için maliyet optimizasyonu yapılmıştır. NMC811 katotlarından yapılan pillerin dört kimya arasında en düşük maliyete sahip olduğu sonucuna varılmıştır. Ek olarak, yüksek menzilli elektirikli araçlar, kg başına maliyet cinsinden en düşük spesifik maliyetlere sahiptir. Üretim hacmindeki veya pil performansı gereksinimlerindeki değişikliklerin optimum tasarım ve üretim maliyetleri üzerindeki etkilerini araştırmak için çeşitli vaka çalışmaları yapılmıştır. Bu çalışmalar sonu-

cunda üretim hacmini artırmanın üretim maliyetini düşüreceği görülmüştür. Katot kalınlığının arttırılması, maliyetlerin düşürülmesi için etkili bir önlemdir. 30 ve 15 dakikalık hızlı şarj, katot kalınlığını sınırlayacaktır.

ACKNOWLEDGEMENTS

First and foremost, I would like to express my gratitude to my advisor, Dr. Tuğçe Yüksel, for her guidance, patience, and unwavering support throughout my master's degree study. It was an honor to have the opportunity to be enlightened by her research experiences, which helped me to develop myself as a researcher and guided me to a solid career plan. My appreciation goes to Prof. Dr. Serhat Yeşilyurt, Assoc. Prof. Dr. Burak Kocuk and Assoc. Prof. Dr. Onur Taylan for agreeing to join my thesis defense jury. My sincere thanks go to them for sharing their valuable knowledge and comments on my thesis, which assisted me in the completion of it. I would like to thank Sabanci University for providing me with the privilege and opportunity of completing my master's studies.

I want to thank my lab mates, Mirmeysam Rafiei, Peiman khandar, Andisheh Chopani, Kazi Sher Ahmad, and Ece Kurt for all the support and good memories. As well as the moral support I received from my closest friends, Nazli Shahbazi, Sina Khalilvandi Behrouzyar, Suzan Behrouzbaraghi, and Sadaf Zarrin cannot be overstated. It would be impossible for me to bear with the hard times without the one and only Faraz Ganjdoust's endless support and kindness. In the end, I want to thank my family for their endless support and love, and for providing the means for me to become who I am now.

I dedicate my thesis to my parents, my sister, and Faraz.

Table of Contents

List of Tables

List of Figures

Chapter 1

INTRODUCTION

This chapter introduces Lithium-ion batteries (LIBs) used in electric vehicles, approaches to the cost modeling of their production, and our motivation for this study. An overview and classification of electrified vehicles are provided. Next, there is a detailed literature review on the discussion of LIB technologies, cost modeling, and design optimization which we consider the main objectives of this thesis. The thesis objectives and contributions will be explained in this chapter.

1.1 Lithium-ion batteries for electrified vehicles

According to the International Energy Agency's (IEA) recent report [4], in 2023 electrical vehicles (EV) have a share of 25% in the European passenger car market. EVs are becoming one of the significant elements of smart cities while concerns about their limited driving range, high costs, and long charging time still create a barrier for these vehicles to lead the transportation market.

EVs are divided into four main categories. Battery electric vehicle (BEV) propulsion completely relies on their battery and electric motor, as a result of that, they require high battery capacity in order to have an acceptable driving range at a single charge. On the other hand, Plug-In Hybrid Electric Vehicles (PHEV) have both conventional internal combustion engine and electric motor that operates separately. Their electric motor is fed by the battery and the battery is charged by an external electric source. In Hybrid Electric Vehicles (HEV) an internal combustion engine is combined with an electric motor to provide propulsion. The combination type of the engine and the motor can be in different types such as series, parallel, etc. Despite the PHEVs, HEVs rely only on their combustion engine power and regenerative braking for charging their batteries. Fuel Cell Electric Vehicles (FCEV) use

hydrogen and oxygen as the fuel and the fuel cell feeds an electric motor with electricity for propulsion [5]. The two latter vehicle types will not be discussed in this thesis because their battery does not engage significantly in the overall cost of the vehicle due to its small capacity.

Generally for PHEVs and EVs batteries, LIB technology has been the primary choice for a long time. LIBs are made of numerous components. The smallest element of a LIB which identifies its specifications is the battery cell. Cells can be connected in series or parallel configurations to form a greater component, a battery module. Finally, a full battery pack will consist of several modules with series/parallel connections, a thermal management unit, and a battery management system (BMS). Cells are composed of two electrodes, a positive electrode (cathode) and a negative electrode (anode), which exchange lithium ions through an electrolyte. Additionally, each cell has a separator to prevent electrical current flow inside the cell and positive and negative electrode current collectors to facilitate electron transfer [6]. These cells can be manufactured in several shapes such as cylindrical, pouch, and prismatic [7]. Figure 1.1 shows the detailed schematic within a pouch cell. The details of the battery cell, module, and pack design used in this study will be explained in the following chapter.

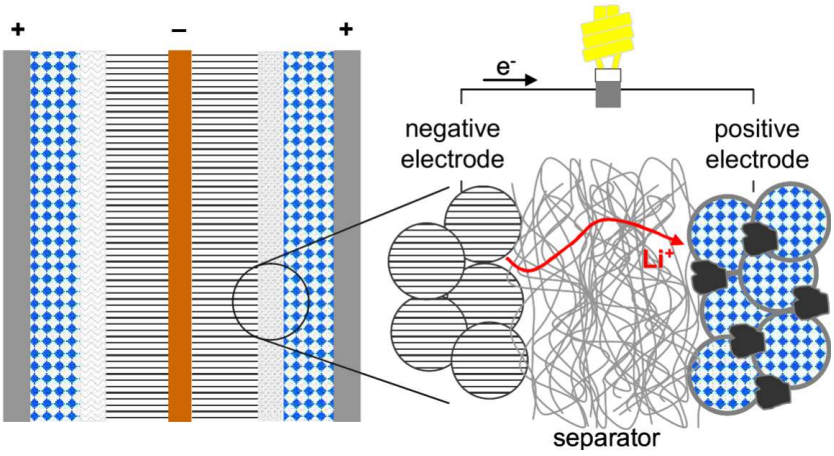

Figure 1.1: Detailed schematic within a pouch cell [3].

1.2 Lithium-ion battery cost modeling

At the end of 2022, the BloombergNEF [8] reported the average price of LIBs for EVs to be $151 per kWh. The LIB price range starts from the lowest of $138 per kWh for BEVs up to $345 per kWh for PHEVs. These prices are not expected to decrease lower than $100 per kWh before 2026 [9]. Since lithium-ion batteries are the most cost-intensive component of EVs, reducing the cost of LIBs is a huge concern for both academia and industry [2], [10]. According to IEA [4] in 2022, cell manufacturing costs increased due to the increased material costs. To be more specific, cathode chemistry is a dominant indicator of the total cost of a lithium-ion battery. In recent years, a few chemistries such as lithium nickel cobalt manganese oxide (NMC), lithium nickel cobalt aluminum oxide (NCA), and lithium iron phosphate (LFP) succeeded to dominate in the EV market. Also, there are new chemistries with promising values for possible lower cost and higher lifespan such as NMC955 [11]. Despite these new emerging technologies, with the current prominent chemistries, it is also possible to achieve the cost targets by optimizing the production and design of the cells. Several electrode manufacturing cost-reducing attempts can be done such as saving the inactive materials by improving quality control, optimizing the processing method for manufacturing the cathode, fastening the slow electrode processing steps, and increasing the coating areas. It is believed that taking such measurements will be effective to decrease the cell manufacturing costs over time [12], [13], [14].

Researchers and LIB manufacturers are making massive efforts each year to develop accurate cost models and cost predictions for these batteries. Argonne National Laboratory (ANL) is the pioneer in developing an open-access LIB design and cost model named Battery Performance and Cost Model, BatPaC [3]. They developed their model in Microsoft Excel spreadsheets, in which prismatic stiff pouch lithium-ion cells with different positive electrode chemistry options were used for the design and cost modeling of battery production for a baseline plant. They have been updating their model according to the latest technologies since 2012. BatPaC was used as a base model in several studies.

An innovation made by Sakti et al. [2] changed the direction of LIB manufacturing cost modeling. They introduced a process-based cost model (PBCM) instead of using scaling factors used in BatPaC or previous studies. They conducted a techno-economic analysis that calculated battery performance, material, and manufacturing costs for a pouch cell design with an NMC cathode and a graphite anode. Input

variables such as equipment cost and processing rates were adopted from BatPaC. The study provided a detailed explanation of the individual production steps and presented the input variables in tables. Their optimization design variables were cathode width, cathode thickness, number of bi-cell layers in each cell, number of cells per module, and the number of modules per pack. They solved a linear optimization problem developed in Microsoft Excel. The study shows that, in addition to cathode material, cathode thickness can also affect the pack cost significantly, especially for high-energy cells, thicker electrodes can reduce pack costs. Another unique approach was made by Nelson et al. [7] while they performed another case study centered around BatPaC, where they compared the standard manufacturing plant with a flexible plant design that could produce LIBs for four types of vehicles at several production volume levels for two different cathode chemistries only in the case of vehicle batteries having the same width and length, all types can be manufactured using the same equipment. They concluded that in such a flexible plant, significant cost savings can occur by producing LIBs for HEVs with different energy capacities due to savings in equipment investment and production time with high production rates for electrode manufacturing processes. On the other hand, they established that there is no remarkable difference in production costs of LIBs with high energy capacities for EVs in a flexible plant compared to a dedicated plant. There is also an ongoing debate on which type of cell should be used for certain applications. A comparison study on cylindrical and prismatic cell designs show that, for large, high-energy LIBs, prismatic cell design can be more efficient due to their geometric design [15]. This may be the reason for most of the original equipment manufacturers (OEM) to change their cell design to prismatic cells. These cells will also be used in this study. Despite all these efforts done by researchers, it is observed that generally experts' predictions of BEV cost are higher than the prices reported by the BEV manufacturers. A comparison study of a PBCM and 12 experts' assessment of LIBs cost forecasts for PHEVs and BEVs for 2018 proves this argument. The underlying reason for this cost prediction difference can be either the technical researchers' and consultants' limited knowledge of the details of the manufacturing and pricing process or the pricing of batteries lower than their real cost by the manufacturers in order to gain a market share in the competitive EV market. Furthermore, it is predicted by all experts that manufacturing costs will continue to decrease as time goes on, however, they claim a sharper cost decline slope for BEV batteries in comparison to PHEVs [16]. In a recent study, efforts have been made to develop a detailed design of a high-capacity NMC battery packs with a silicon nanowire (SiNW) anode for next-generation lithium-ion battery (NG LIB) technologies in electric vehicle (EV) applications by utilizing BatPaC. The results

indicate that this technology has cost and mass advantages compared to commercial NMC-Graphite cells [17].

Battery optimization is not limited only to BEVs, there have been several studies on PHEVs batteries due to their high power demand and different performance requirements from BEVs. Since the optimization design variables for batteries can be continuous such as cell dimensions or integer such as the number of bi-cell layers, a special optimization approach should be carried out. For instance, Xue et al. [18] used a hybrid gradient-based and gradient-free optimization method to find an optimized battery design for PHEVs. Their goal was to minimize the volume, mass, and cost of the battery. However, their battery and cost model was initially designed for an ideal electrochemical cell model and they converted it to a pack-level model. The study needs improvements on the cell model and manufacturing constraints. In 2022, Epp et al. [19] published a paper based on cost and weight optimization of high voltage LIBs involving only battery module size and positioning within the battery pack as design parameters. They conducted their research for different cell forms and sizes and concluded that cells with lower costs can result in high-cost battery systems. Their study confirms the importance of evaluating different cell formats from a system-based perspective. In some applications and for certain vehicles, a particular cell geometry is better than others.

Another concern in the field of LIBs is the capability of fast charging. Battery technology of the future should combine a long lifespan with high energy and power density, enabling long-range travel as well as quick recharge anywhere, under any weather condition. As a consequence of the physics of each of these requirements, there are trade-offs; for example, thicker electrodes that are required for high energy density are more severely affected by the concentration and potential gradients that are generated when the battery is fast-charged. In order to minimize the effect of fast charging on battery life, manufacturers apply some electrode manufacturing limitations [20]. Song J et al. [21] conducted experimental research on the fast-charging capabilities of LIBs. They coupled a 3-D thermal model with two 1-D electrochemical Newman models to apply a constant-risk charging protocol to minimize the charging time. They developed a fast-charging model which is a function of charging time, maximum allowable temperature, cell geometry, and area-specific impedance (ASI) at 50% SOC. They concluded that charging protocols such as maximum allowable temperature, charging C-rate (A measure of the rate at which a battery is charged to its maximum capacity), and anode potential have critical effects on charging time and cell cost. They determined that increasing the maximum temperature will allow the user to decrease the charging time by 50%. Finally,

increasing the allowable C-rate from 4C to 12C can be a great advantage for thin anodes with a thickness of 40 mm or less. This is because the influence of other design limits is minimized at this thickness, allowing for a dramatic decrease in charging time by 67%.

Considering the literature review explained in this chapter, some research gaps have been identified which are listed below:

- Generally a comprehensive cell to pack level design optimization has not been done.
- The effects of designing high voltage battery on production costs have not been investigated.
- For cost optimization purposes, PBCM have not been used commonly in the literature.
- The effects of designing batteries with fast charging capability on manufacturing costs have not been investigated.

1.3 Thesis Objectives and Contributions

EV battery costs account for a large portion of the total price of an EV. As a result, LIB cost optimization studies are in high demand. The objective of these studies was generally to optimize the production cost of the battery or cell, with a few limited decision variables related to the overall design of the battery, such as pack/module sizing or pack mass. In order to fill the research gaps mentioned before, this study is done inspired by the earlier studies [3], [2], [22] and considering the existing research gap, we developed a comprehensive battery pack manufacturing cost optimization problem. Moreover, we aim to reconstruct this optimization problem as a tool in MATLAB. This tool has the capability to determine the LIB design with the minimum production cost by defining the performance requirements and the characteristics of the LIB manufacturing plant such as the building and labor costs and the overall costs and operation characteristics of the manufacturing equipment. Because of the tool's parametric structure, it can be adjusted to any factory's production techniques and parameters. In this way, the manufacturer will be able to estimate the effects of the plant characteristics, annual labor hours, and battery pack design on the final product cost. This tool can be useful to design the battery and estimate the product cost before building a LIB manufacturing plant

or for predicting the effects of a change in the production line on the final product cost of an existing plant.

The objectives of this thesis are to **propose an optimization strategy to minimize the production cost of the LIB that can satisfy the performance requirements.**

To meet this objective, the main contributions of this thesis are listed below:

- Established a process-based cost model that can calculate battery manufacturing costs considering the design requirements.
- Developed a user-friendly tool in the MATLAB environment that is able to find the optimal design of a Lithium-ion battery pack with minimum production cost.
- Investigated the effects of several parameters such as vehicle size, cathode chemistry, voltage levels, and charging requirements of a battery pack on its production cost.

1.4 Thesis Outline

The thesis is organized as follows:

- **Chapter 2** describes the optimization problem and the general approach to solving the problem. Then the battery pack manufacturing process and battery pack model assumptions are explained in detail. Since a process-based cost model is used in this thesis, a brief introduction to this model is provided in this chapter.
- Each case study assumption and the simulation results are provided and discussed in **Chapter 3** The benefits of all obtained designs from optimization are evaluated based on different application purposes.
- Finally, **Chapter 4** of the thesis summarizes the findings of the thesis and concludes with recommendations for future work.

Chapter 2

Battery Cost Optimization Problem

In this chapter, the optimization problem, the process-based cost model, and the overall principles of the battery model is demonstrated.

2.1 Optimization Problem

An optimization problem is defined to minimize the production cost of Lithium-ion batteries for electrified vehicle applications. The problem is defined as follows:

$$\text{Minimize } C(\mathbf{x}) \tag{2.1}$$

$$\text{w.r.t} \quad \mathbf{x} = [x_t, x_b, x_w, x_s, x_{mpr}, x_r, x_{cp}]$$

$$\textit{subject to:} \begin{cases} P^{\text{Req}} - P(\mathbf{x}) \leqslant 0 & \text{(2.1a)} \\ E^{\text{Req}} - E(\mathbf{x}) \leqslant 0 & \text{(2.1b)} \\ c^{\text{MIN}} \leqslant c(\mathbf{x}) \leqslant c^{\text{MAX}} & \text{(2.1c)} \\ V^{\text{MIN}} \leqslant V(\mathbf{x}) \leqslant V^{\text{MAX}} & \text{(2.1d)} \\ \mathbf{x}^{\text{MIN}} \leqslant \mathbf{x} \leqslant \mathbf{x}^{\text{MAX}} & \text{(2.1e)} \\ L^{\text{bat}}(\mathbf{x}) \leqslant L^{\text{MAX}} & \text{(2.1f)} \\ W^{\text{bat}}(\mathbf{x}) \leqslant W^{\text{MAX}} & \text{(2.1g)} \\ x^{\text{R}} = \{x_t, x_w\} \in R & \text{(2.1h)} \\ x^{\text{I}} = \{x_b, x_s, x_{cp}, x_{mpr}, x_r\} \in Z & \text{(2.1i)} \end{cases}$$

C($\mathbf{x}$) is the battery pack production cost calculated by a process-based cost model which will be explained in the following section. x_t is the cathode thickness, x_b is the number of bi-cell layers, x_w is the cathode width, x_s is the number of series cells in a module, x_{cp} is the cells in parallel, x_{mpr} is the number of modules per row, and x_r is the number of rows of modules. x_{mpr} and x_r indicate the physical configuration of the modules within the pack. All modules are assumed to be connected in series for simplified calculations. $c(\mathbf{x})$ is the cell capacity in Ah which should be within the minimum and maximum bounds of c^{MIN} and c^{MAX}. $V(\mathbf{x})$ is the total battery pack voltage which should be between V^{MIN} and V^{MAX}. $E(\mathbf{x})$ is the energy capacity of the battery which should meet the required energy capacity, $E^{\text{Req}}(\mathbf{x})$. Also, the pack power should be equal to or higher than the pack power requirement, $P^{\text{Req}}(\mathbf{x})$. Battery pack dimensions must be lower than the pack size limits which are L^{MAX} and W^{MAX}. The upper and lower boundaries for all decision variables and performance requirements are given in Table 2.1. Cathode thickness and cathode width are continuous and the number of bi-cell layers, number of series cells per module, cells in parallel, number of modules per row, and number of rows of modules are integer. Each decision variable must be within its bounds.

The optimization problem can be defined as Mixed Integer Non-linear Integer Programming (MINLP). To solve this problem *fmincon* function from the MATLAB optimization toolbox was used. *fmincon* is a gradient-based solver that can use different algorithms to find a local minima. In order to increase the chance of approaching to a global minima, we tested randomized multi-starts for identifying the initial start points. We used different initialized points to solve the optimization problem. The optimization problem approaches similar solutions with each different initial point. A relaxed non-integer solution is found as an initial continuous solution for the optimization problem. Then, the integer decision variables of an optimized design (the best solution obtained by our approach) are found by enumeration of these variables inside their boundaries.

Table 2.1: Boundaries for design variables and constraints for BEVs and PHEVs

	x_t [μm]	x_b	x_w [mm]	x_s	x_{mpr}	x_r	$c(\mathbf{x})$ [Ah]	$V(\mathbf{x})$ [v]	Pack length [ft]	Pack width [ft]
Minimum	15	1	1	1	1	1	10	PHEV: 100 BEV: 240	-	-
Maximum	120	50	1000	30	50	4	68	400	5	5

The boundaries are generally obtained by the recent trends in battery manufacturing or by the default assumption from BatPaC 5.0 [3]. Energy and power requirements for each vehicle type are given in Table 2.2.

Table 2.2: Pack energy and power requirements [1] and [2]

Vehicle type	PHEV30	PHEV60	BEV200	BEV300
Energy requirement (kWh)	8	16.5	59	92
Power requirement (kW)	44	47.9	125	200

Cell capacity function, $c(\mathbf{x})$, battery pack energy, $E(\mathbf{x})$, and battery pack power, $P(\mathbf{x})$, are provided in Equations 2.2 to 2.5, respectively:

$$c(\mathbf{x}) = \frac{x_t\, A^{\mathrm{P}}(\mathbf{x})(s^{\mathrm{PAM}}\, m^{\mathrm{FR}} \rho^{\mathrm{P}})}{10^9} \tag{2.2}$$

s^{PAM} is the specific capacity of positive electrode active material, m^{FR} is the mass fraction of the active material in the positive electrode and ρ^{P} is the positive electrode density. $A^{\mathrm{P}}(\mathbf{x})$ is the positive electrode active area, defined as:

$$A^{\mathrm{P}}(\mathbf{x}) = 2\, x_b\, r\, x_w^2 \tag{2.3}$$

where r is the cell's length/width ratio. Moreover,

$$E(\mathbf{x}) = x_{cp}\, x_s\, x_{mpr}\, x_r\, v^{\mathrm{NOM}} c(\mathbf{x}) \tag{2.4}$$

where v^{NOM} is the nominal cell voltage, and

$$P(\mathbf{x}) = \frac{x_{cp}\, x_s\, x_{mpr}\, x_r\, v^{\mathrm{OCV,P}}\, v^{\mathrm{OCV,FR}} (1 - v^{\mathrm{OCV,FR}})\, A^{\mathrm{P}}(\mathbf{x})}{x_t\, R(\mathbf{x})^{\mathrm{ASI}}} \tag{2.5}$$

where $v^{\mathrm{OCV,P}}$ is the open-circuit voltage at the state of charge (SOC) for rated power (20% for BEV and 80% for PHEV), $v^{\mathrm{OCV,FR}}$ is the fraction of the open circuit voltage while the designed power is achieved which is a default value of 0.8 taken from BatPaC, and $R(\mathbf{x})^{\mathrm{ASI}}$ is the area-specific impedance ($\Omega\mathrm{cm}^2$). $R(\mathbf{x})^{\mathrm{ASI}}$ is dependent on numerous parameters which will be discussed in section 2.3. Its new value for each node is calculated directly in the cost function. The cost function is explained in the section 2.2. After finding a relaxed non-integer solution, we need to find integer solutions for x^{I}. Enumeration is used to find the best design with

integer values for x^{I}. All possible combinations of the integer decision variables which yield feasible solutions are calculated and listed. The combination that gives the minimum cost is selected as the optimized solution. The relationship between the x_b and x_w decision variables is in a way such that the best solutions are found at a specific positive electrode area. Because of this reason during the enumeration, we fix the positive electrode area to the value which is found by the continuous solution and we enumerate the x_b according to this value, then we calculate x_w corresponding for each x_b. The optimized design with minimum cost is selected within the feasible solutions regarding the constraints. The algorithm used by fmincon is the sequential quadratic problem (SQP) method. A quadratic subproblem is approximated at each iteration by the SQP method assuming the design space near the optimum to be convex. Each quadratic subproblem's solution is then used to begin the next iteration.

The optimization algorithm is explained in Table 2.3.

Table 2.3: Optimization algorithm

1. Solve {2.1: 2.1a - 2.1g } where x^{I} are real numbers
2. Enumerate for x_b while $x_b {x_w}^2 = Constant$
3. Enumerate for x^{I} to generate a list of integer x^{I} within the boundaries
3. Compute $C(\mathbf{x})$ for each x group from the enumeration list
4. Find the minimum $C(\mathbf{x})$ value that satisfies the constraints and return the corresponding x

2.2 Process-based cost model

The cost of manufacturing a product or technology can be modeled in several ways. A variant-based and a generative cost estimation approach can be distinguished within the existing cost estimating methods. The variant-based cost estimation takes into account the similarity of the product under consideration to previously manufactured products. A previously manufactured product's cost can serve as a guide for the new product cost estimation. A relatively standard product can be manufactured using this method in small and medium batches. However, the generative cost estimation is based on the assumption that the costs of manufacturing

a product are influenced by the operations required [23]. We realize that variant-based cost accounting methods cannot forecast the cost of new designs, materials, or architectures, hence they are inadequate for our purposes. The process-based cost modeling method is a generative cost estimation approach for evaluating different technological choices in the decision-making process. This method is used to model material flow and calculate the costs associated with each process step. Moreover, it can be utilized to perform sensitivity analysis for one or more parameters which can alter the final cost [24].

We developed our PBCM based on the approach introduced by Sakti et al. [2]. Based on process-level data, a PBCM estimates the amount of capital, labor, materials, and energy required to achieve production targets for a definite design. It is possible to produce both acceptable and faulty units at each process step, so earlier process steps must produce additional units for the final step to yield sufficient acceptable units. Using the following formula for the effective production volume, the requirements for each component are calculated taking into account the yield of each process step.

$$v_{i-1} = \frac{v_i}{y_i(\mathbf{x})} \quad \forall i \in \{1, 2, ..., n\} \tag{2.6}$$

where v_i is the effective production volume output at step i in a year, v_{i-1} is the input production volume required at step i, y_i is the yield rate at corresponding step. n indicates the total number of production steps. In the steps which have yield rates other than one, the effective production volume output also varies with respect to design parameters. The cell stacking yield is assumed to be 95% and the solvent recovery step yield is taken as 99.5% according to BatPaC 5.0 [3]. The process steps of the manufacturing plant are adjusted according to BatPaC 5.0 as it is shown in Figure 2.1.

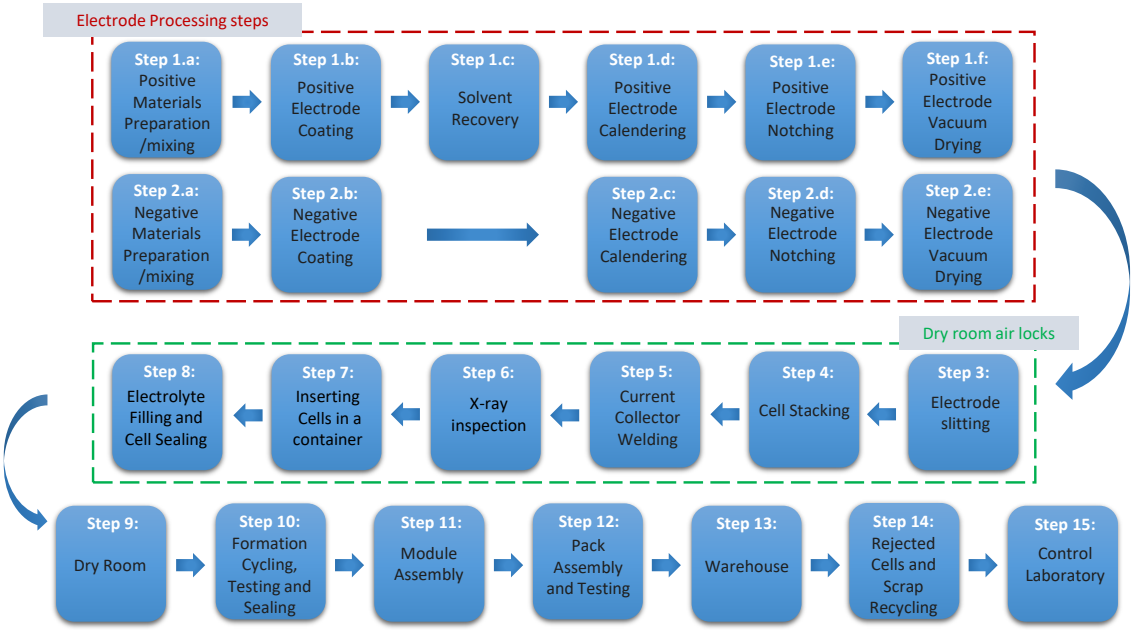

Figure 2.1: Battery manufacturing steps

The cost function can be defined as:

$$C(\mathbf{x}) = \frac{C^{\mathrm{MTL}}(\mathbf{x}) + C^{\mathrm{EQP}}(\mathbf{x}) + C^{\mathrm{BLD}}(\mathbf{x}) + C^{\mathrm{LBR}}(\mathbf{x}) + C^{\mathrm{ERG}}(\mathbf{x}) + C^{\mathrm{AUX}}(\mathbf{x}) + C^{\mathrm{MNT}}(\mathbf{x}) + C^{\mathrm{OH}}(\mathbf{x})}{v_n} \tag{2.7}$$

where $C^{\mathrm{MTL}}(\mathbf{x})$ is the annual material cost, $C^{\mathrm{EQP}}(\mathbf{x})$ is the capital equipment cost, $C^{\mathrm{BLD}}(\mathbf{x})$, $C^{\mathrm{LBR}}(\mathbf{x})$, $C^{\mathrm{ERG}}(\mathbf{x})$, $C^{\mathrm{AUX}}(\mathbf{x})$, $C^{\mathrm{MNT}}(\mathbf{x})$, $C^{\mathrm{OH}}(\mathbf{x})$ corresponds to the annual building, labor, energy, auxiliary equipment, maintenance and overhead costs, respectively. v_n is the production volume which refers to the number of battery packs produced annually. Each of the functions mentioned in equation 2.7 is a function design $\mathbf{(x)}$ and time required to manufacture the target number of battery packs. $C^{\mathrm{MTL}}(\mathbf{x})$ is obtained by calculating the total mass of required active material for each electrode and other materials used for each component such as aluminum, copper, bus bars, etc. Active material costs can differ depending on their cobalt, nickel content, and other parameters. The costs for the material used in this study are provided in Table 2.5. $C^{\mathrm{EQP}}(\mathbf{x})$ is calculated by obtaining the ratio of target production for each step to the unit production capacity of each step. In most of the steps, the number of machines should be natural numbers. So, we calculate the minimum number of equipment for each step to satisfy the production requirement of that step. These steps are tagged as dedicated. For the steps in which we do not have an accurate discrete processing rate or they have continuous processing

nature, we assign non-dedicated tags. It means these steps may not have an integer number of machines. $C^{\mathrm{BLD}}(\mathbf{x})$ and $C^{\mathrm{LBR}}(\mathbf{x})$ are determined by the total number of required equipment, their footprint, and required process time. Also, building costs and labor wages directly affect these costs. In our study, we assumed 3000 $ per m^2 for the building floor cost and 25 $ per hour for the labor wage according to the latest BatPaC. The underlying assumption for the base case in this study is an annual production volume of 500,000 packs. The total annual work days are assumed to be 320 days with 3 working shifts. $C^{\mathrm{ERG}}(\mathbf{x})$ is directly calculated by the labor and material costs. The remaining costs are a function of equipment and building costs. All the assumptions and costs are taken from BatPaC 5.0 and explained in the following equations [3]. In Table 2.4, all fixed parameters used for cost calculations are given. The values are taken from BatPaC and Sakti et al [3], [2].

Table 2.4: Fixed parameters for cost calculation

Input	Values	Units
Working days per year ($\mathrm{t}^{\mathrm{DPY}}$)	320	days/year
Number of hours with no shifts (t^{NS})	0	h/day
Unpaid breaks (t^{UB})	2	h/day
Paid breaks (t^{PB})	1	h/day
Building space cost ($\mathrm{p}^{\mathrm{BLD}}$)	3000	$/m^2
Direct wage ($\mathrm{p}^{\mathrm{LBR}}$)	25	$/h
Discount rate (d)	10	%
Capital recovery period (j $\in J_i^{\mathrm{EQP}}$)	6	years
Building recovery period (j $\in J_i^{\mathrm{BLD}}$)	20	years
Auxiliary equipment cost (γ^{AUX})	10	% of main machine cost
Maintenance cost (γ^{MNT})	10	% of main machine cost
Fixed overhead cost (γ^{OH})	35	% of other fixed costs
Energy cost (γ^{ERG})	3	% of material and labor costs

All the following cost equations can be calculated by using the values given in Tables 2.4 and 2.6. The cost calculation equations are taken from [2].

$$N_{ij}(\mathbf{x}) = \begin{cases} \left\lceil \dfrac{t_i^{CYC}\, v_i(\mathbf{x})}{t^{\mathrm{DPY}}(24 - t^{\mathrm{NS}} - t^{\mathrm{UB}} - t^{\mathrm{PB}} - t_i^{\mathrm{UD}})} \right\rceil & \forall i \in S_D, j \in J_i^{\mathrm{EQP}} \\ \dfrac{t_i^{CYC}\, v_i(\mathbf{x})}{t^{\mathrm{DPY}}(24 - t^{\mathrm{NS}} - t^{\mathrm{UB}} - t^{\mathrm{PB}} - t_i^{\mathrm{UD}})} & \forall i \in S_{ND}, j \in J_i^{\mathrm{EQP}} \\ \dfrac{t_i^{CYC}\, v_i(\mathbf{x})}{t^{\mathrm{DPY}}(24 - t^{\mathrm{NS}} - t^{\mathrm{UB}} - t^{\mathrm{PB}} - t_i^{\mathrm{UD}})} L_i & \forall i \in S, j \in J_i^{\mathrm{LBR}} \end{cases} \tag{2.8}$$

where N_{ij} indicated the number of machines or laborers, S_D is the set of dedicated steps, $S_N D$ is the non-dedicated steps and S stands for all the dedicated and non-dedicated steps. J_i^{EQP} is the cost element set for equipment at step i, J_i^{BLD} is the list of building cost elements in step i and, t_i^{UD} is the average unplanned downtime hours per day at step i.

$$C^{\mathrm{EQP}} = \sum_{i=1}^{n} \sum_{j \in J_i^{\mathrm{EQP}}} \phi_{ij}\, p_{ij}^{\mathrm{EQP}} N_{ij}(\mathbf{x}) \tag{2.9}$$

where ϕ_{ij} is the capital recovery factor and can be calculated by Equation 2.10.

$$\phi_{ij} = \frac{d(1+d)^{I_{ij}}}{(1+d)^{I_{ij}} - 1} \tag{2.10}$$

I_{ij} values are given in Table 2.4 as the capital or the building recovery period.

$$C^{\mathrm{BLD}} = \sum_{i=1}^{n} \sum_{j \in J_i^{\mathrm{EQP}}} \phi_{ij}\, p^{\mathrm{BLD}} \theta_{ik} N_{ik}(\mathbf{x}) \tag{2.11}$$

$$C^{\mathrm{LBR}} = \sum_{i=1}^{n} \sum_{j \in J_i^{\mathrm{LBR}}} (24 - t^{\mathrm{NS}} - t^{\mathrm{UB}})\, t^{\mathrm{DPY}}\, p^{\mathrm{LBR}}\, N_{ij}(\mathbf{x}) \tag{2.12}$$

$$C^{\mathrm{ERG}} = \gamma^{\mathrm{ERG}}(C^{\mathrm{MTL}} + C^{\mathrm{LBR}}) \tag{2.13}$$

$$C^{\mathrm{AUX}} = \gamma^{\mathrm{AUX}} C^{\mathrm{EQP}} \tag{2.14}$$

$$C^{\mathrm{MNT}} = \gamma^{\mathrm{MNT}} C^{\mathrm{EQP}} \tag{2.15}$$

$$C^{\mathrm{OH}} = \gamma^{\mathrm{OH}} (C^{\mathrm{BLD}} + C^{\mathrm{EQP}} + C^{\mathrm{AUX}} + C^{\mathrm{MNT}}) \tag{2.16}$$

Table 2.5: Active material costs [3]

Electrode type	Electrode chemistry	Material Cost ($/kg)
Positive electrode	NMC811	26
	NMC622	25
	NCA	26
	LFP	10
Negative electrode	Graphite	10

Each electrode's material is prepared by mixing the active material, carbon, binder, and binder solvent in a mixing machine. The capacity or processing rates of all equipment used in battery manufacturing are listed in Table 2.6. Then, the current collector foil's both sides will be coated with a thin layer of prepared material for each electrode. The coated sheets will be calendared in order to adjust the thickness of the electrode to the desired value. Afterward, the electrode will be cut into two strips in the notching machines. The electrodes contain moisture that should be removed before cell stacking. The remaining moisture may cause harmful reactions inside the cell. Hence, dryer machines should be used to dry the electrodes. The moisture of cathode thickness contains a significant amount of a toxic and expensive material called N-Methyl-2-pyrrolidone (NMP) which should be recycled from the captured moisture of the dryers. Cell assembly should be done inside a dry room to prevent the formation of any moisture inside the cells. The electrodes will be cut into designated sizes. Then, cells will be stacked using the electrodes and separators. The current collector foil ends of positive and negative electrodes will be welded together to create tabs for electrical connections. X-ray inspection will be done to check the alignment of the electrode stacks. After rejecting the faulty cells, the acceptable ones will be inserted inside their containers and filled with electrolyte. The cells

get sealed and they leave the dry room for the next step. In the next step, aging, gas removal, performance testing, formation cycling, final sealing, electrochemical testing, and final inspection is done under the general step name of formation and cycling. It is the most costly and undetermined step in cell manufacturing. It takes long charge/discharge cycling time with several types of machines and it can be extremely variable depending on the manufacturer. The rejected cells will be sent for recycling. Then the accepted cells are assembled inside the modules and the modules are assembled in row racks to be located inside the pack. Finally, the packs will be stored in the warehouse and they will be shipped to their consumers. All assumptions for each step are given in Table 2.6.

Table 2.6: Assumptions for each process step

Step number	Step name	Equipment cost (p_{ij}^{EQP})(M)	Footprint (θ_i)(m^2)	Fractional use of labor (L_i)	Processing rate (t_i^{CYC})$^{-1}$	Unplanned downtime (t_i^{UD})	Dedicated
1.a	Positive electrode materials preparation/ mixing	11.11	450	1.5	2300 l/shift	25%	yes
1.b	Positive electrode coating	18	3200	1.5	80 m/min	30%	yes
1.c	Solvent recovery	36	1100	2	3151* kg/hr	20%	no
1.d	Positive electrode calendering	3.125	262.5	1	100 m/min	30%	yes
1.e	Positive electrode notching	0.85	94.12	1	24m/min	20%	yes
1.f	Positive electrode vacuum drying	2.8	400	1	7000* kg/shift	20%	yes
2.a	Negative electrode materials preparation/ mixing	11.7	367	1.5	2700 l/shift	25%	yes
2.b	Negative electrode coating	15.6	3200	1.5	80 m/min	30%	yes
2.c	Negative electrode calendering	2.8	234	1	100 m/min	30%	yes
2.d	Negative electrode notching	0.85	95	1	24 m/min	20%	yes
2.e	Negative electrode vacuum drying	2.8	400	1	7000* kg/shift	20%	yes
3	Electrode slitting	0.89	-	1	8812* m^2/hr	20%	yes
4	Cell stacking	0.93	-	0.5	2.50 cells/min	20%	yes
5	Current collector welding	7.6	-	1	18 cell/min	20%	yes
6	X-ray inspection	0.56	-	1	18 cells/min	20%	yes
7	Inserting cell in container	0.85	-	0.5	36 cells/min	20%	yes
8	Electrolyte filling and cell sealing	1	-	0.67	18 cells/min	25%	yes
9	Dry room	7.30	61000	200	0.03 m^2/m^2	-	no
10	Formation cycling, testing, and sealing	5.92	785	73	1600* cells/cycle	20%	yes
11	Module assembly	8.6	2455	2	2 modules/min	20%	yes
12	Pack assembly and testing	18.8	5400	4	12 packs/hr	20%	yes
13	Warehouse	200	10000	5	38540* kg/shift	20%	no
14	Rejected cell and scrap recycle	9.3	3300	5	4163* kg/shift	20%	no
15	Control labrotory	16	1300	6	781.25* kWh/hr	20%	no

Notes: The process step rates with a * are taken from BatPaC 3.0 [25] due to the lack of information.

The process step data is taken from BatPaC 5.0 [3].

2.3 Battery model

We based our battery model on BatPaC 5.0 parameters and equations which were based on a Microsoft Excel spreadsheet. BatPac is an Excel-based calculation model developed by Argonne National Laboratory (ANL) rather than an optimization model. We carried out the equations from this model to an optimization model developed in MATLAB environment. Our model is a parametric model which can be modified for new parameters or even with new equations when necessary. Due to the iterative structure of Excel spreadsheets, minor changes were done in the formulation of cell capacity while converting the model to a MATLAB script. The new cell capacity function is taken from Sakti et al. [2]. Each user requirement in BatPaC calculates a different parameter of the cell design. Based on the specific capacity of electrode active materials and cell voltages, the amount of electrode active materials is calculated. The power is calculated by the cell resistance and cell area. After the cell is designed, the module and pack dimensions, mass, and performance will be calculated. As mentioned in Section 2.1, some of the structural design inputs such as the number of cells per module, series/parallel connections, and the number of modules per row are used as decision variables in this study. In this way, the user does not need to make initial assumptions about the aforementioned variables and the optimization model will find the detailed optimum design of the battery pack with the minimum cost. Also, BatPaC uses default scaling factors for calculating the material and production costs of LIBs by comparing the required production volume with their default manufacturing plant with a production capacity of 50 GWh per year. The BatPaCs'cost calculation approach is simplified by the following equation:

$$C = C_0 \left(\frac{R_1}{R_0}\right)^{\mathrm{P}} \tag{2.17}$$

C_0 is the labor, building, or equipment cost of the baseline plant in BatPaC. R_0 is the baseline plant's production rate. R_1 is the required production rate. P is the scale factor which is less than 1 for most of the process steps implying that production rates and costs are not directly proportional. More details on P values and BatPaC baseline plant can be found in the BatPaC user manual [3]. However, we concluded that scaling the production volumes of each step may yield a low-accuracy calculation if the design parameters are changed significantly from BatPaC's baseline assumptions. Hence, we used a PBCM with the data taken from the BatPaC. Inputs and outputs of BatPaC and thesis approach are defined precisely in Table 2.7. It

is clear that we have made significant changes in the inputs and outputs of our model compared to the BatPaC. The design of the battery and its components are explained in detail in this section.

Table 2.7: Main input, outputs of BatPaC and thesis approach

	BatPaC [3]	Thesis approach
Inputs	**Structural** - Cell thickness - Electrode length/width ratio - Number of cells per module - Series/parallel connections - Number of modules per row - Terminal and bus bar dimensions **Performance:** - Pack energy and power - SOC range - Fast charging time **Cell chemistry:** - Electrode, separator and current collector characteristics	- Electrode length/width ratio - Pack energy target - Pack power target - Fast charging time - SOC range - Electrode, separator and current collector characteristics
Outputs	- Electrode thickness and coating area - Number of bi-cell layers - Cell/module/pack mass and volumes	- Electrode thickness and coating area - Number of bi-cell layers - Number of cells in modules - Number of modules per row and number of rows of modules - Cells series/parallel connections - Final pack energy, power, voltage - Cell capacity - Pack size, volume, mass

2.3.1 Cell design

The cell electrodes are constituted by covering metal current collectors with composite materials consisting of active materials, binders, and carbon conductors. For the negative electrode, both sides of copper foils are covered by active materials. The active material covers both sides of aluminum foils to construct the positive electrode. Finally, a separator with a larger area than the electrodes should be placed between electrodes to avoid short circuits and performed as a self-shutdown

system at high temperatures by melting. This composition is called a bi-cell layer. A lithium-ion cell is built by adding several bi-cell layers until it reaches the desired capacity. Finally, all layers are inserted into aluminum containers with a polymer coating and they will be filled with electrolytes. Current collectors are welded together to be connected to the positive and negative tabs. These tabs are stretched out of the pouch structure to provide electrical connections [3]. The explained cell's schematic is shown in Figure 2.2.

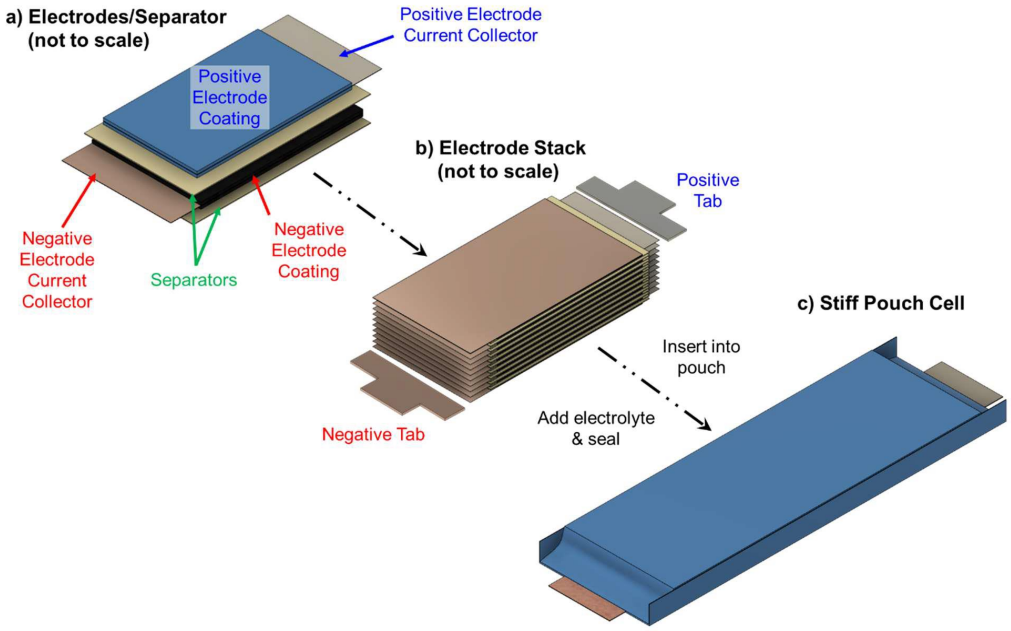

Figure 2.2: Stiff pouch cell components [3]

2.3.1.1 Cell chemistries

Generally, manufacturers choose graphite as the active material for negative electrodes. In recent years, silicon additives are also being used to increase the energy density of active materials by some companies. According to the global EV Outlook 2023 by the IEA, around 70% of the electrodes in the market are made of graphite and silicon-doped graphite electrodes contribute to the remaining share along some other chemistries [4]. In this research, only graphite-based anodes are considered in the study cases and the effect of silicon additives for anodes on pack cost and design can be examined in future work. In contrast to negative electrodes, there are numerous preferences for positive electrode active materials depending on battery application. For this study, we will be comparing four different cathode active material chemistries, NMC811 (Lithium nickel manganese cobalt oxides), NMC622,

NCA (lithium nickel cobalt aluminum oxides), and LFP (lithium iron phosphate). The numbers in NMC chemistries indicate the molar ratio of each element. Each of these chemistries has its own significant characteristics. Generally, the manufacturers chose the cathode chemistry according to the battery pack application. The specifications of each chemistry are shown in Figure 2.3 [26].

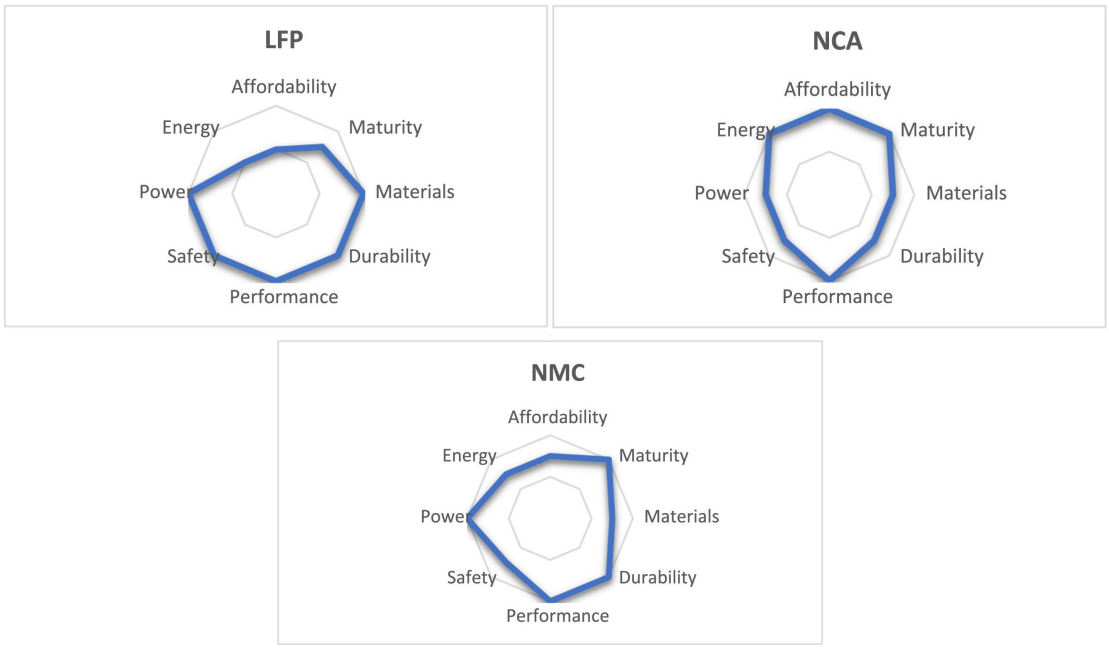

Figure 2.3: Cathode chemistry trade-offs

These active materials have different specific capacities which are listed in Table 2.8.

Table 2.8: Active material specific capacities from BatPaC 5.0

Electrode type	Electrode chemistry	Active material specific capacity (mAh/g)
Positive electrode	NMC811 ($LiNi_{0.8}Mn_{0.1}Co_{0.1}O_2$)	214
	NMC622 ($LiNi_{0.6}Mn_{0.2}Co_{0.2}O_2$)	191
	NCA ($LiNi_{0.8}Co_{0.15}Al_{0.05}O_2$)	202
	LFP ($LiFePO_4$)	157
Negative electrode	Graphite	360

2.3.1.2 ASI calculation

ASI is not a constant value for cell design or chemistry. Equation 2.5 indicates that it is a critical parameter in determining pack power and it is highly dependent on the cell and pack design. Hence, ASI is modeled by design parameters to provide us the accurate pack power for our optimized design. Cell resistance is a complex combination of resistances caused by physical processes taking place over a variable period of time. It can depend on many factors such as charge/discharge pulse length, SOC, charge/discharge pulse length, current density, particle size, etc. $R(x)^{\mathrm{ASI}}$ can be defined as in equation 2.18.

$$R(\mathbf{x})^{\mathrm{ASI}} = R^{\mathrm{echem}} + R^{\mathrm{CC}} + R^{\mathrm{CellTerm}} + \frac{R^{\mathrm{CNCT}} A^{\mathrm{P}}}{x_{cp}\, x_s\, x_{mpr}\, x_r} \tag{2.18}$$

where R^{echem} is electrochemical processes ASI and is a function of the temperature. R^{CC} is the current collector foil impedance. It is a combination of resistances for coated and uncoated areas of the electrode foils. R^{CellTerm} is related to the resistance of the cell terminals and R^{CNCT} is an impedance caused by the the cell terminals, module terminals, module interconnects, and battery terminals. A^{P} is the positive electrode area. Electrochemical ASI is calculated by the equation 2.19.

$$R^{\mathrm{echem}} = R^{\mathrm{Const}} + R^{\mathrm{Pos}} + R^{\mathrm{Neg}} \tag{2.19}$$

R^{Pos} and R^{Neg} are positive and negative electrode interfacial impedances. They can be modeled using the interfacial charge transfer resistance by the equations 2.20 - 2.22.

$$R^{\mathrm{Neg}} = \frac{R^{\mathrm{GAS}}\, T_{ref}}{i_o\, \alpha\, \delta_{Neg}\, F} \tag{2.20}$$

where R^{GAS} is the universal gas constant, F is the Faraday's constant, T_{ref} is the reference temperature (298.15 K), i_o is the exchange current density and α is a parameter related to the active material particle radius and volume fraction of the active material. δ_{Neg} is the negative electrode thickness which can be calculated by the equation 2.21.

$$\delta_{Neg} = r^{\mathrm{NP}} \frac{s^{\mathrm{NAM}} \rho^{N}}{s^{\mathrm{PAM}} \rho^{P}} \tag{2.21}$$

where r^{NP} is the negative to positive electrode ratio, s^{NAM} is the negative electrode active material capacity and ρ^{N} is the negative electrode density. Also R^{Pos} is calculated as:

$$R^{\mathrm{Pos}} = \frac{R^{\mathrm{GAS}} T_{ref}}{i_o \alpha x_t F} \left[\left(1 - \frac{I^{\mathrm{MAX}}}{I^{\mathrm{ionic,lim}}}\right) \left(1 - \left(\frac{I^{\mathrm{c}}}{I^{\mathrm{c,lim}}}\right)^{2}\right) \right]^{-0.5} \tag{2.22}$$

where I^{MAX} is the C-rate at full power, $I^{\mathrm{ionic,lim}}$ is the limiting ionic current for lithium cation transport through the separator, I^{c} is the maximum current density at full power and $I^{\mathrm{c,lim}}$ limiting current density. R^{Const} is obtained by the default electrochemical ASI. It is a constant value to define any impedance that could not be defined with the other parameter. R^{CNCT} is defined in equation 2.23.

$$R^{\mathrm{CNCT}} = R^{\mathrm{CNCT,cell}} + R^{\mathrm{CNCT,mod}} + R^{\mathrm{CNCT,pack}} \tag{2.23}$$

2.3.1.3 Fast charge model

Electrodes with high thicknesses may suffer from concentration and potential gradients during fast charging under high current densities. This gives us the motivation to find a fast-charging model to investigate its effects on the design and cost of the battery. We utilized a fast-charging model which is taken from BatPaC to find a relation between electrode thickness and fast charging time. The maximum electrode thickness in a cell that can achieve the desired charge time is calculated by an empirical correlation according to the operational limits. BatPaC used an electrochemical-thermal model to develop the correlation for electrode thickness. The formulation of calculating the maximum allowable thickness for the fast charging is given below:

$$x_{t_{FC}} = \frac{\alpha\, ln^2(t_{chg}) + \beta}{s^{\mathrm{PAM}}\, \rho^{\mathrm{p}}} \tag{2.24}$$

t_{chg} is the desired charging time in minutes, α and β are functions of design parameters shown in equation 2.27. A group of Pearson and Kendall correlations were used to find the dominant parameters that affect the α and β.

$$\{\alpha, \beta\} = f(L, T_{max}, R(\mathbf{x})^{\mathrm{ASI}}_{10s,50\%}) \tag{2.25}$$

Where L refers to the cell length and $R(x)^{\mathrm{ASI}}_{10s,50\%}$ is the reference area-specific resistance of the cell at ten seconds and 50% state of charge (SOC). T_{max} is the maximum allowable temperature. The user can identify the cell thickness for fast charging by defining the maximum allowable temperature and reference ASI. α and β are obtained from the following equations.

$$\alpha = \alpha_1 + \alpha_2\, L^2 + \alpha_3\, T_{max} \tag{2.26}$$

$$\beta = \left(\beta_1\, L + \beta_2\, T_{max}\, L + \beta_3\, T_{max} + \beta_4\, T^2_{max}\right) \frac{R(\mathbf{x})^{\mathrm{ASI}}_{10s,50\%}}{12.5} \tag{2.27}$$

α_i and β_i are fixed values taken from BatPaC 5.0.

2.3.2 Module design

Modules are formed by placing cells together inside a steel module enclosure with thermal conductors between them to manage the temperature of the cells. This enclosure also contains cell interconnects and a module management system. The advantages of placing cells in modules instead of locating them directly inside the pack are improved safety and cell status monitoring, easier manufacturing, and simplified pack sizing. Then, modules are placed in compartments called row racks. This structure is used to enhance the system mechanically and avoid any pressure

on the cells. Also, some coolant panels are placed inside row racks for thermal management purposes. Since they are in direct contact with the liquid coolant, stainless steel is a good option for these layers to avoid corrosion. Module component breakdown and the module placement in row racks are shown in Figure 2.4 and Figure 2.5. Module interconnects shown in Figure 2.5 demonstrate a series module connection which is also used assumed in our battery model.

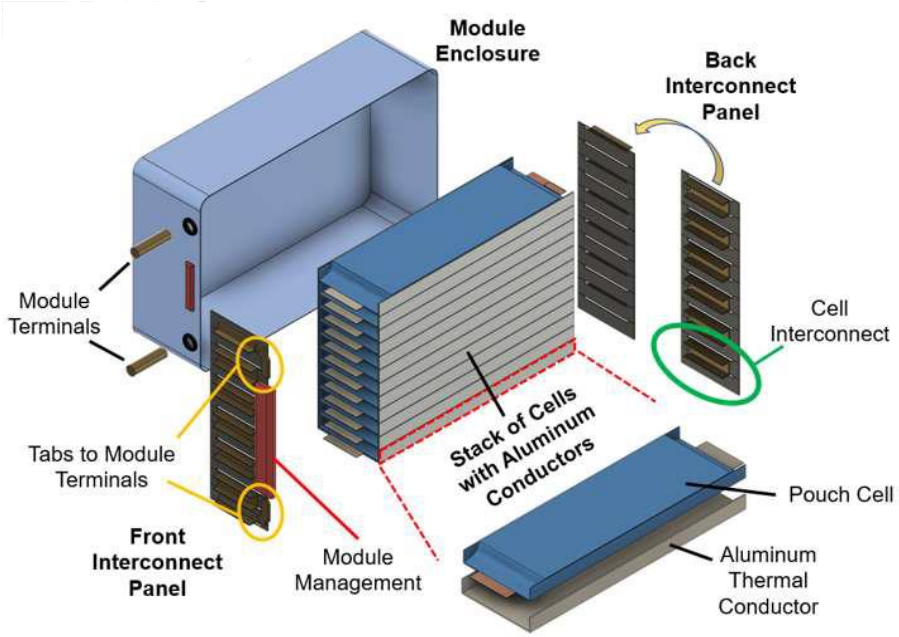

Figure 2.4: Battery module components [3]

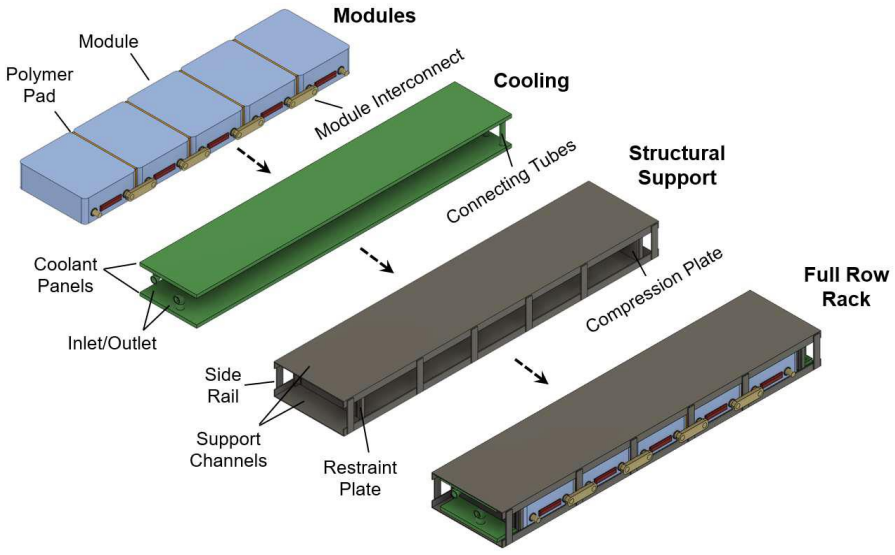

Figure 2.5: Module row racks [3]

2.3.3 Pack design

The battery pack consists of module row racks, coolant tubes, BMS, a thermal management system, module bus bars, and terminals. The mass and volume of the BMS and thermal management system are calculated but their location inside the pack depends on the manufacturer's precise vehicle design. The pack's package is made of aluminum metal sheets. The bottom part is reinforced with steel layers to protect it from any sort of mechanical damage. The steel part is slightly larger than the battery pack size. The number of bus bars depends on the number of row racks. In the BatPac user manual, it is explained that packs with 1, 2, and 4 rows of modules will require 0 or 1 bus bars and they are the most efficient designs. Hence, we set our optimization model boundaries for rows of modules accordingly. Another limiting factor for our design can be the pack size. The battery pack should be suitable to be fitted in a typical sedan vehicle. The pack dimensions must not exceed 5 feet. Moreover, it was mentioned by the BatPaC creators that connecting more than two modules in parallel may result in an underestimation of module-to-module interconnection length. For simplification, we assumed having one module in parallel in our calculations. Figure 2.6 shows the pack components and their general schematic.

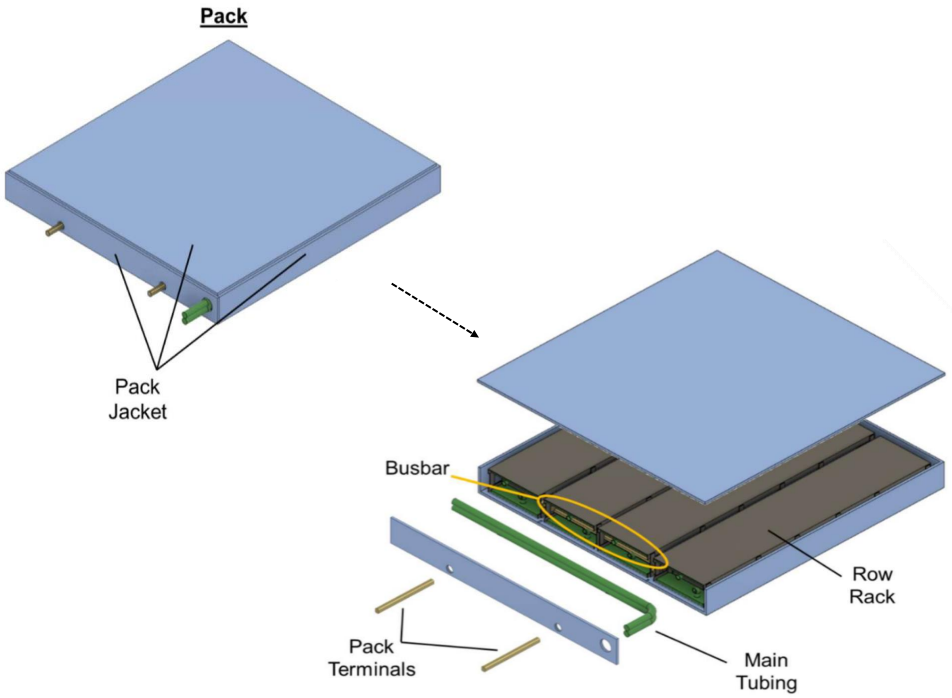

Figure 2.6: Battery pack components [3]

Chapter 3

Computational Experiments and Results

Several case studies are performed in order to investigate different battery production scenarios. The effects of various factors such as electrode design, battery performance constraints, and production volumes on the battery production costs and optimized design suggestions by our model are explored and compared in this chapter.

3.1 Computational experiments

As it was mentioned in Table 2.3, first, a continuous optimized design was found for each case by the MATLAB optimization toolbox. Then enumeration was performed to find the integer values for x^{I}. Finally, the design with the minimum cost which satisfies all the constraints was selected as our optimized battery design for the base case. Later, several case studies were performed to examine the effects of the new assumptions on the overall cost, specific cost, and design parameters. All case studies and their particular assumptions are mentioned in Table 3.1.

3.2 Results

The results of each case study are discussed in the following subsections.

Table 3.1: Case studies and assumptions

Parameters	Cases				
	Base	Relaxed boundaries	High voltage	Production volume change	Fast charge
Upper boundaries[1]	[120,50,1000,65,30,4,4]	[200,50,1000,100,30,4,4]	Base	Base	$[x_{t_{FC}}, 50, 1000, 65, 30, 4, 4]$[2]
Voltage	240-400 (V)	240-400 (V)	600-800 (V)	240-400 (V)	240-400 (V)
Cell capacity	10-68 (Ah)	10-120 (Ah)	10-68 (Ah)	10-68 (Ah)	10-68 (Ah)
Charging time	Not considered	Not considered	Not considered	Not considered	15 minutes 30 minutes
Annual production volume	500,000	500,000	500,000	100,000 750,000	500,000

Notes:

1: $\mathbf{x} = [x_t, x_b, x_w, x_s, x_{mpr}, x_r, x_{cp}]$

2: $x_{t_{FC}}$ = Maximum allowable cathode thickness values are provided in Table 3.6.

3.2.1 Base case

Optimized design variables for each vehicle type and chemistry are given in Tables 3.2 and 3.3. Mainly, the optimized design with the lowest cost for all chemistries will have the highest cathode thickness possible except for PHEV30. PHEV30 requires a relatively small battery, and as a result of that the optimum design can be found without increasing the cathode thickness up to the upper boundary. Additionally, in LFP chemistry results, it is observed that even PHEV30 requires a 120 μm cathode to meet the requirements. Table 2.8 in Chapter 2 indicates that LFP chemistry has the lowest specific capacity. Hence, high cathode thickness for this chemistry is an expected result. There is a trend of enlarging the cathode width and decreasing the number of bi-cell layers as pack energy capacity increases. Also, the total number of cells in series increases with the pack size, which is an expected result. There is a common trend of having more cells per module instead of having more modules in series. The higher costs of module interconnections compared to cell interconnections [3] explain this choice. This trend is also observable in some recent pack configurations such as recent BYD batteries [27]. In general, LFP chemistry will require the most and NMC811 will require the least number of cells in total due to their specific capacity differences. From Table 3.2 it is seen that for PHEV30 the optimum point exists on the intersection of minimum pack power and energy constraints lines. On the other hand, for larger PHEVs and BEVs, pack energy

constraint is the limiting factor because the optimized design is found slightly above the energy requirement. Pack voltage is found within the boundaries of all vehicles. The cell connection type plays a critical role in adjusting the overall pack voltage. Regulating the pack voltage will only be feasible by changing the cells' series/parallel connection types. For PHEVs, lower voltages are preferable since higher voltages will require designs with more cells with higher costs. For BEVs, more parallel connections are preferred to limit the pack voltage. Cell capacity is limited by the upper bound for all vehicles. It is an expected result because packs with large cell capacities will require less number of cells and cell/module interconnections resulting in lower costs. Pack size is designed to fit inside a passenger vehicle. Long-range BEVs demand larger pack sizes.

Although the total costs for BEVs are the highest, their specific cost is lower due to their high energy capacities. In general, specific energy tends to decrease by increasing the energy of the pack. In the bigger packs, the costs of battery management and thermal management units are spread over a greater pack energy capacity. From Table 2.5 it was expected to have LFP as the cheapest design however, the highest costs are reported for LFP and the lowest belong to NMC811. This trend is due to the high number of cells in LFP designs.

Table 3.2: Battery pack performance parameters and dimensions of optimized designs for base case

	Pack energy (kWh)	Pack power (kW)	Pack voltage (V)	Cell capacity (Ah)	Pack length (mm)	Pack width (mm)
NMC811						
PHEV30	8.08	44.03	113.8	68.0	243.94	537.25
PHEV60	16.66	65.89	117.34	68.0	410.41	536.09
BEV200	59.08	234.24	277.36	68.0	667.58	1011.2
BEV300	92.91	354.49	327.15	68.0	891.56	1076.3
NMC622						
PHEV30	8.06	44.05	114.88	68.0	255.04	530.95
PHEV60	16.62	72.71	118.47	68.0	394.95	560.08
BEV200	60.46	265.14	287.2	68.0	654.61	1059.2
BEV300	92.71	406.72	330.28	68.0	962.35	1059.2
LFP						
PHEV30	8.13	51.99	118.15	68.0	293.19	567.09
PHEV60	16.73	104.74	121.43	68.0	485.26	588.08
BEV200	59	359.37	285.53	68.0	1393.4	612.67
BEV300	92.24	579.83	334.76	68.0	1201.4	1115.2
NCA						
PHEV30	8.04	44.67	113.02	67.99	258.57	520.93
PHEV60	16.60	66.33	116.55	68.0	405.97	542.56
BEV200	60.36	241.86	282.56	68.0	674.65	1024.1
BEV300	92.56	370.98	324.94	67.99	993	1024.1

Table 3.3: Base case results

	Cathode Thickness (μm)	# of bi-cell layers	Cathode width (mm)	# of series cells per module	# of modules per row	# of rows of modules	# of cells in parallel	Pack cost ($)	Pack specific cost ($/kWh)
NMC 811									
PHEV30	83.6	10	141.9	32	1	1	1	2377.3	294.25
PHEV60	120	7	141.6	33	1	1	2	3424.4	205.5
BEV200	120	7	141.65	39	1	2	3	9041.6	153
BEV300	120	6	153	46	1	2	4	13332	143.48
NMC 622									
PHEV30	96.86	10	139.5	32	1	1	1	2413	299.30
PHEV60	120	7	149.8	33	1	1	2	3517	211.5
BEV200	120	7	149.8	40	1	2	3	9571	158
BEV300	120	7	149.8	46	1	2	4	13891	149.8
LFP									
PHEV30	120	11	151.2	36	1	1	1	2475	304
PHEV60	120	10	158.6	37	1	1	2	3670	219.4
BEV200	120	9	167.2	29	3	1	3	9855	167
BEV300	120	10	158.6	51	1	2	4	14484	157
NCA									
PHEV30	85.3	11	136.1	32	1	1	1	2403	298.6
PHEV60	120	7	143.8	33	1	1	2	3475	209.3
BEV200	120	7	143.8	40	1	2	3	9421	156
BEV300	120	7	143.8	46	1	2	4	13641	147.4

3.2.2 Relaxed upper boundaries

For LIB manufacturing, current technologies may not be sufficient for further production cost reduction of LIBs. As mentioned before, increasing the thickness of positive electrodes is one of the effective measures to reduce the cost of a LIB cell. However, manufacturing cathodes with thicknesses higher than 100-125 μm requires special manufacturing techniques or may have durability problems [2]. Moreover, high electrode thickness limits the charging and discharging capabilities of the LIB. With the current status of LIB manufacturing and the characteristics of commercial chemistries, this approach may not be applicable. However, research on special electrodes such as semi-solid cathodes has shown that electrode thickness can be increased up to 2mm [28] which is not suitable for the purpose of our research. Also, a tendency for manufacturing cells with higher capacities is evident. At the moment, some OEMs such as SAMSUNG SDI are manufacturing cells with capacities as high as 94Ah for BEVs [29]. Furthermore, BYD company has been a pioneer in manufacturing blade LFP batteries for their BEVs [27]. These batteries have a cell-to-pack level design which means they do not have any modules connected in series/parallel. This design has the advantage of space reduction. This trend has raised the question of whether blade batteries can become the future design choice of battery manufacturers without considering the current safety and maintenance technologies. Because of these reasons, we conducted a case study with relaxed upper boundaries for cell capacity, cathode thickness, and number of series cells in a module in order to investigate the possibilities of cost reduction for near-future technologies. Optimized design with minimum cost has been calculated for all vehicle types and all four chemistries. The specific cost of each optimized design for both the base case and the relaxed case is demonstrated in Figure 3.1 for better observation.

It is observed that for all cathode chemistries, the specific cost of LIB has decreased compared to the base case. The increased cathode thickness upper bound allowed us to choose a thicker electrode. For easier comparison, we select the two extreme results, the LFP and NMC811 chemistries. The computational results for electrode thickness for LFP will vary from $148\,\mu m$ for PHEV30 up to $200\,\mu m$ for BEV300. Since the design has a higher cathode thickness compared to the base case, it will require fewer cells in general to satisfy performance constraints. So the costs are lower compared to the base case. From the cathode-chemistry perspective, LFP requires high cathode thickness due to its low active material capacity. Hence, it will increase the cathode thickness of the optimized design up to the upper bound which

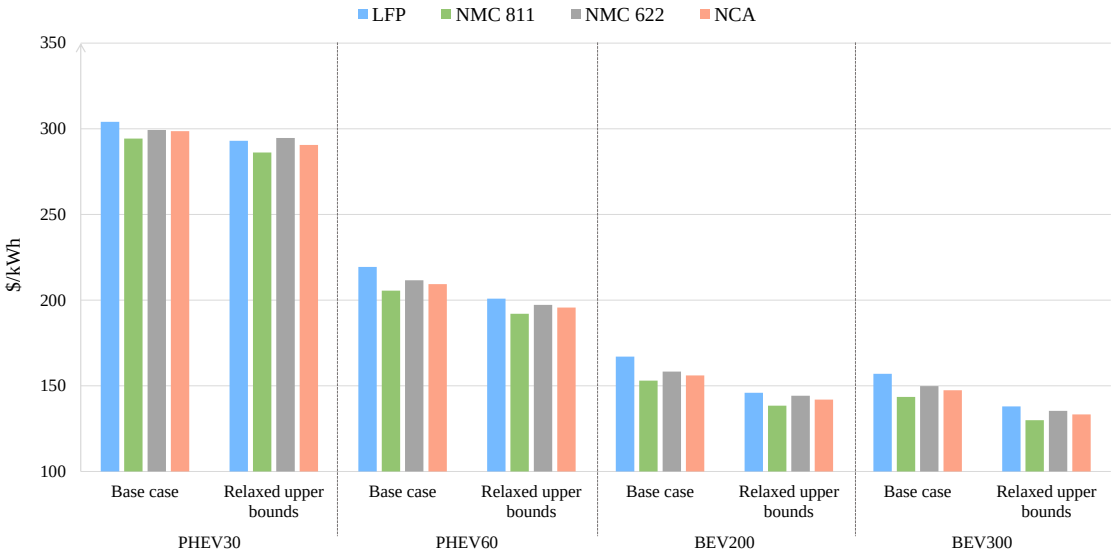

Figure 3.1: Comparison of specific costs of optimized designs for the base and the relaxed cases

is 200 μm for big batteries. For NMC811 the optimized design values of cathode thickness change between 82 μm and 163.6 μm. The results of this chemistry for PHEV30 are the same as the base case in Table 3.3. This means that for small PHEVs, electrodes made of energy-dense materials such as NMC811 from Table 2.8 with moderate thicknesses can satisfy the performance requirements, and increasing the electrode thickness further will increase the cost of the product. Additionally, the optimized design for the relaxed case requires total cells remarkably less than the base case. This enables us the decrease the production cost even more. The main similarity of optimized design for all chemistries and vehicles was the cell capacity. Cell capacity was chosen to be the highest possible value which was 120 Ah in this case study. The underlying reason is the benefit of designing the battery with larger capacity cells and less number of cells in total. The detailed results of optimized design and other performance characteristics of the battery are provided in the appendix A.

3.2.3 High voltage

It is recommended that the battery voltage of electric vehicles be increased from 400 to 800 volts in order to improve charging time. Under the same current, 800 volts batteries tend to be charged faster than 400 volts batteries. Additionally, high voltages can result in reductions in conduction losses, wiring size, and vehicle mass.

The 800-V system is currently being used in several high-end electric passenger vehicles [30] [31]. One of the research gaps in LIB cost studies was inspecting the effects of designing high voltage (HV) batteries on production costs for long-range BEV applications. We performed a case study on this aspect to fill the current research gap. The voltage constraints are set to new values mentioned in Table 3.1 to design HV battery packs. The optimized specific cost for all chemistries and BEV types are demonstrated in Figure 3.2.

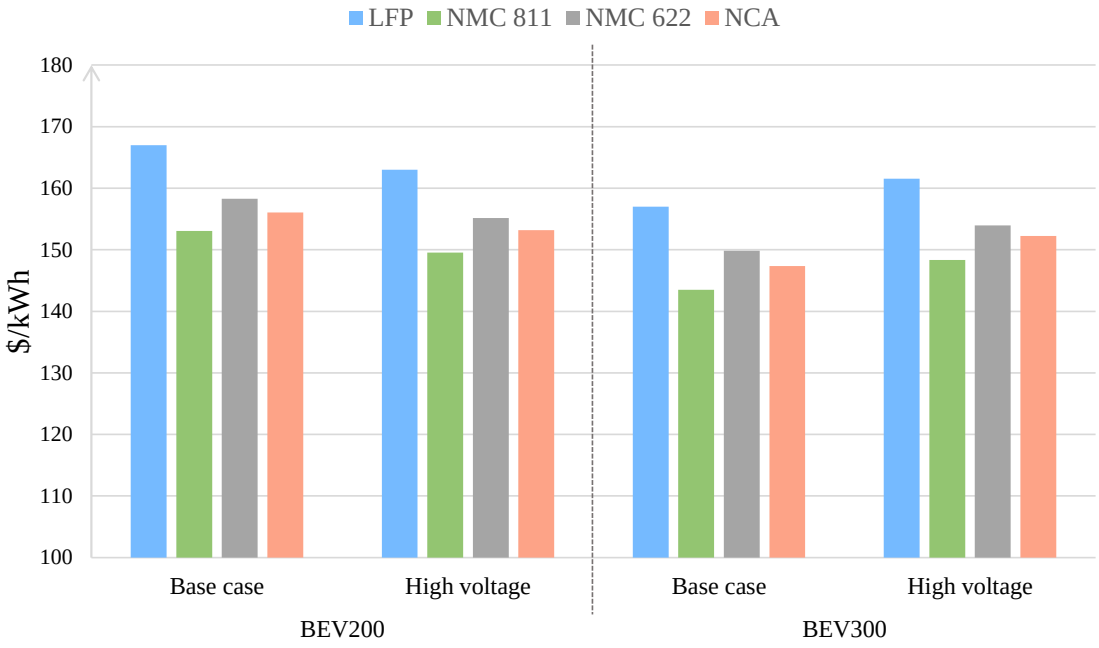

Figure 3.2: High voltage battery specific cost results

Table 3.4: Design parameters results from optimization for high voltage batteries

		Cathode thickness (μm)	# of bi-cell layers	Cathode width (mm)	# of series cells per module	# of modules per row	# of rows of modules	# of cells in parallel
NMC 811	BEV200	120	6	152.9	17	5	2	2
	BEV300	120	5	167.6	61	3	1	2
LFP	BEV200	120	10	158.6	46	2	2	2
	BEV300	120	10	158.6	51	2	2	2

The results indicate that for BEV300 designing a higher voltage battery pack results in higher specific costs. In contrast, for BEV200 high voltage pack design results in a lower specific cost. To investigate this inconsistency in more depth, we analyzed

the total pack cost and other optimized result parameters. The reported total costs in Table 3.5 indicate that for both BEVs the total pack cost has increased. In other words, high voltage design has a remarkable effect on the total cost of a relatively smaller battery. In Figure 3.3, the higher voltage levels of this case compared to the base case were expected. Pack energy is higher than the required energy for BEV200 and pack voltage is equal to the lower voltage limit which is 600 volts. By comparing the results in Tables 3.3 and 3.4, we realize that for BEV200 in the optimized results, the number of total cells are increased unreasonably to meet the voltage constraint and consequently, the energy capacity will be surplus for the requirements. This indicates that designing a high voltage BEV battery with a range of 200 miles may not be feasible with our power and energy requirements. As a results of that, the designed battery will have a higher range than 200 miles. In addition, the cathode width is also increased for high-voltage batteries. This will have a direct effect on the production cost of the electrodes. In conclusion, although designing high-voltage batteries can increase production costs, from performance perspective it can be beneficial to design such batteries.

Table 3.5: Comparison of total pack costs for the base case and high voltage case

	Base case	High voltage case
BEV200	9041.6 $	12839 $
BEV300	13332 $	13707 $

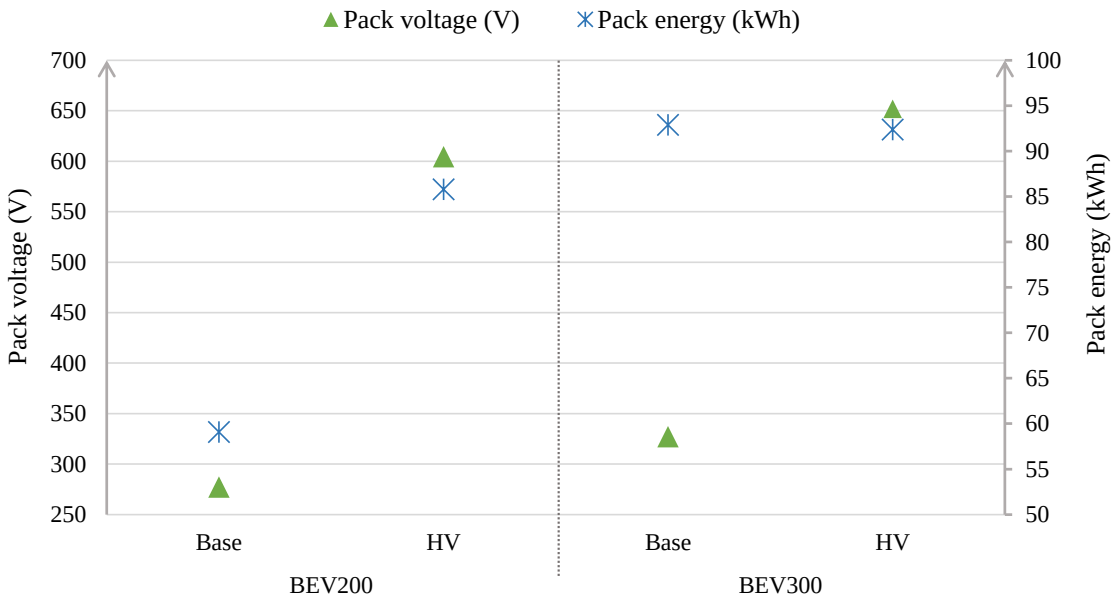

Figure 3.3: High voltage battery power and energy

3.2.4 Production volume

From the equation 2.7, it is seen that by increasing the annual production volume, the production cost of each battery pack will decrease. However, this relationship is not linear due to the characteristics of the cost function. We studied the manufacturing plants with three different production volumes. Figure 3.4 demonstrates the results for four types of vehicles. The most affected production cost belongs to PHEV30. It can be explained as producing small batteries in small volumes are not cost-effective. Building a plant with high processing rates and big equipment require high production volumes. In general, for the PHEV30 case, it is required to purchase only 1 machine for each dedicated processing step which may not operate at full capacity. This will increase the production cost. A suggestion for this problem is to increase the production capacity or convert the plant to a flexible plant with several battery products. In order to investigate this trend further, the cost breakdown for manufacturing a PHEV30 battery in 100,000 and 500,000 packs per year is established in Figure 3.5

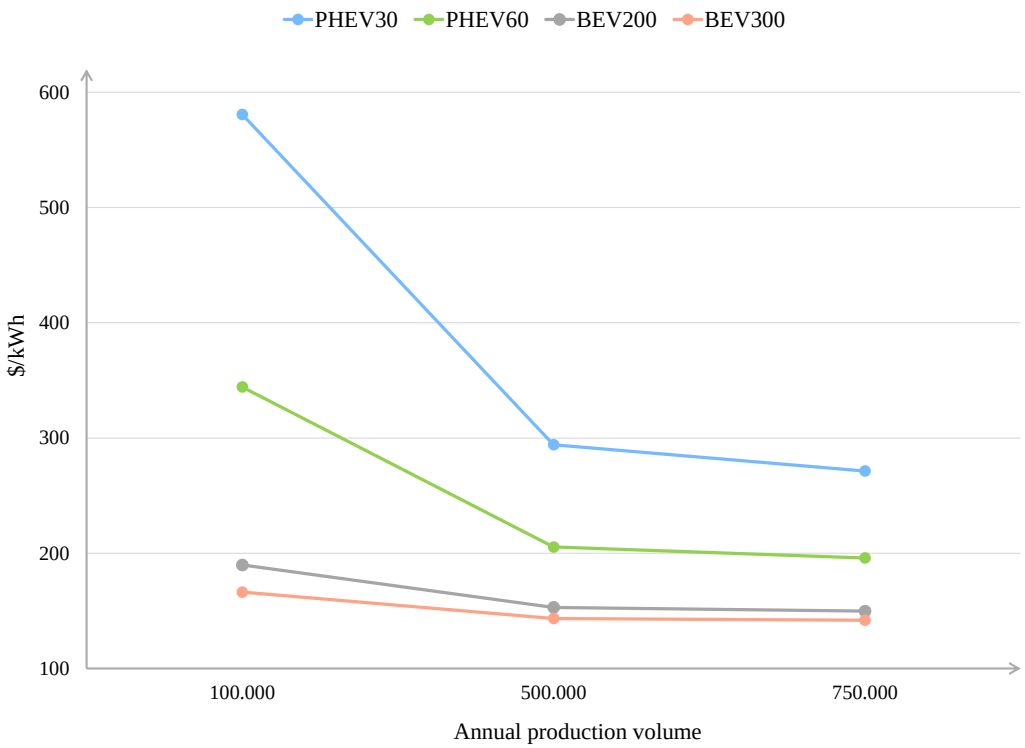

Figure 3.4: Comparison of specific costs for different annual production volumes

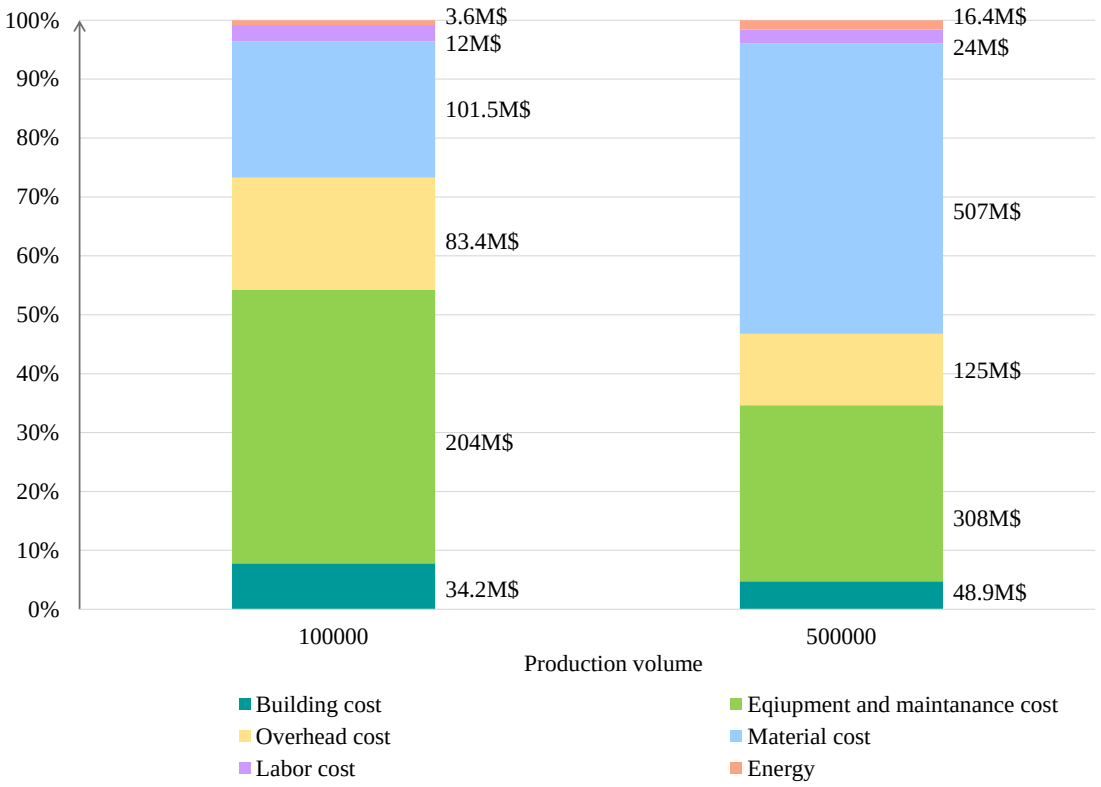

Figure 3.5: Cost breakdown for 100,000 and 500,000 annual production of PHEV30 battery packs

From Figure 3.5 it is observed that the share of the material cost increases proportionally by increasing the production volume. On the other hand, equipment costs and the costs related to the equipment costs contribute will have decreased shares in the overall cost.

3.2.5 Fast charging

The long charging time of BEVs and not having sufficient charging stations decreases the traveling range for many BEV users. In recent years, the fast charging capability of the LIBs has served as the opportunity for BEVs to compete with conventional internal combustion engine vehicles. Fast charging can be done on several levels. DC fast charging level 2 and Tesla's DC superchargers enable the user to charge the battery of BEVs up to 80% SOC in 20 minutes [32]. One of the US Advanced Battery Consortium's goals for 2023 was to commercialize low-cost fast chargers with the capability of 80% SOC charging in 15 minutes. 30-minute fast charging option already exists in many BEVs. Batteries should be manufactured accordingly

for fast charging. As mentioned in Chapter 1, the limiting factor of fast charging is the cathode thickness. We conducted a case study for examining the outcomes of producing LIBs qualified for 30 and 15-minute fast charging. In the base case, the maximum allowable cathode thickness for each fast charging time is calculated and demonstrated in Table 3.6. Then, the cathode thickness upper bound is set to these values, and a new optimized design with minimum cost is found.

Table 3.6: Calculated maximum allowable thickness for fast charging

		Maximum allowable cathode thickness (μm)		
		1 hour fast charge	30 minutes fast charge	15 minutes fast charge
NMC811	BEV200	161.11	108.22	65.12
	BEV300	162.57	109.23	65.76
LFP	BEV200	148.62	99.61	99.61
	BEV300	150.65	101.01	60.54

As shown in Figure 3.6, limiting the cathode thickness will result in increased specific costs for BEVs. For the 30-minute case, the cost difference is not as significant as the 15-minute case. The major reason for this trend is the minor difference between calculated cathode thicknesses for 30-minute fast charging and the base case maximum cathode thickness. For example, as shown in Table 3.6, the maximum cathode thickness which can enable 30-minute fast charge for BEV200 was calculated as 108 μm, and for 15-minute fast charge, it was found to be 65 μm which is half of the allowable thickness for the base case. Hence, we conclude that special electrodes should be designed for fast charging times of less than 20 minutes.

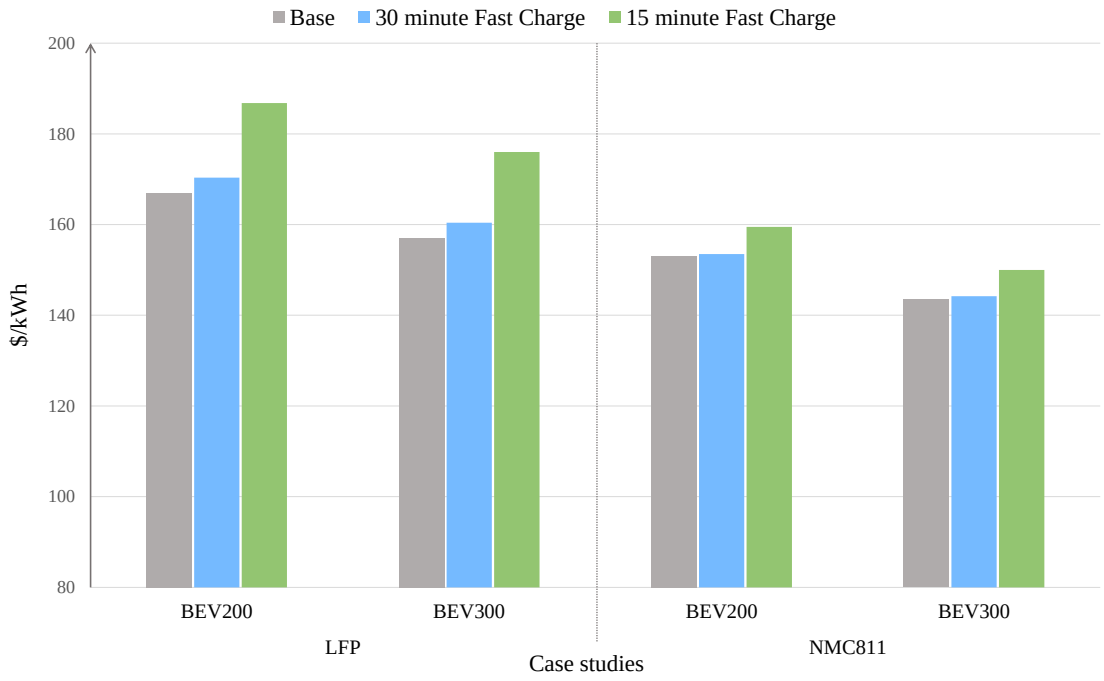

Figure 3.6: Specific costs of LIBs with fast charging capability

3.2.6 Summary of the case studies

For a better conclusion, all case studies for NMC811 are demonstrated in Figure 3.7. The grey bar indicates the base case specific cost for BEV200 and BEV300. It is seen that fast charging in 30 minutes compatibility does not affect the specific cost of the battery. However, enabling 15-minute fast charging can increase the cost of the battery due to the cathode thickness limitation. High voltage batteries will have a higher specific cost generally. The BEV200 results oppose this trend due to increased pack energy. Relaxation of the upper boundaries tends to lower production costs by choosing fewer cells with large capacities and positive electrode thicknesses. The variations in annual production volume do not affect the specific costs linearly as reported in the literature [2]. Increasing the production volume will not have a remarkable impact on the production cost of the battery after a certain level.

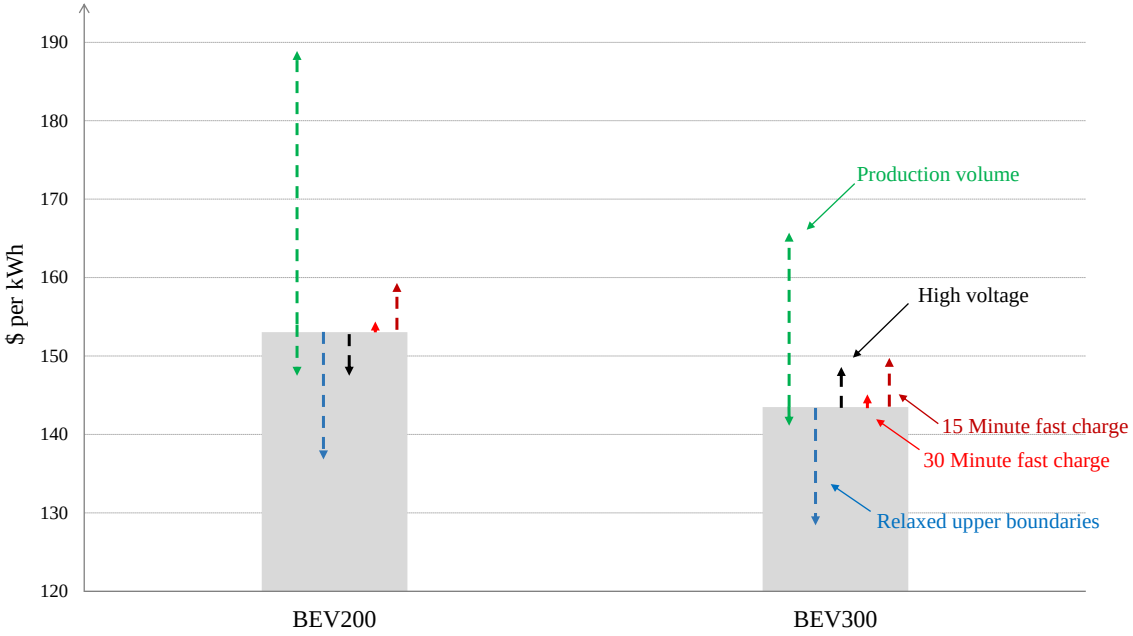

Figure 3.7: Summary of all case studies for NMC811

Chapter 4

Conclusion and Recommendations

4.1 Concluding Remarks

This study presents an approach to the cost optimization of lithium-ion batteries. The main aim of this study is to calculate the optimized design for LIBs with minimum manufacturing costs.

We developed a battery model in MATLAB based on BatPaC 5.0 parameters and equations. The base case assumptions rely on the recent trends in LIBs used for BEVs and PHEVs. After implementing the battery model, a process-based cost model (PCBM) developed by Sakti et al. [2], was refined pursuant to recent manufacturing data taken from BatPaC 5.0. Costs of materials, labor, equipment, floor, and processing rates are updated. After defining the new PBCM, an optimization problem is introduced. The optimization problem aims to minimize the total cost of a battery pack and return the optimized design that satisfies all the requirements. Seven decision variables were chosen according to their impact on the LIB performance and cost. Since some of these decision variables must be integers, this problem becomes mixed-integer non-linear programming (MINLP). To solve this problem, first, a continuous solution was found by utilizing the MATLAB optimization toolbox. Next, enumeration was done for the integer variables to find an optimized solution with the minimum cost. This battery optimization tool is a parametric tool and it can be adjusted according to the user's desired manufacturing plant. The investors of a battery manufacturing plant can utilize this tool to investigate the cost-effectiveness of new or already existing manufacturing techniques.

In order to broaden our research domain, we conducted several case studies for four different chemistries: NMC811, NMC622, NCA, and LFP. It is concluded that in

general, BEVs have lower specific costs in $/kWh compared to PHEVs. This is due to the high energy capacities of BEVs, which results in high-efficiency production of LIBs. In general, the specific cost decreases by increasing the production volume. Moreover, we concluded that large plants with massive equipment and high processing rates may be oversized for producing small PHEV batteries, causing high specific production costs. Generally, the minimum cost is obtained by the thickest cathode thickness possible and the highest cell capacity within the limits. The high voltage case study indicates that designing such batteries is only feasible for high energy and power applications. In order to minimize the degradation and lithium plating effects of fast charging, the positive electrode thickness must be limited. Such designs will have lower electrode thickness and higher specific costs. Relaxing the upper boundaries of some decision variables resulted in optimum designs with more cells per module and fewer modules. Since LFP has a low active material capacity, the designs made of this chemistry will require more cells in total to achieve the requirements. This trend causes LIBs made of LFP cathodes to have higher specific costs, despite their low active material prices per kilogram. On the other hand, energy-dense chemistries such as NMC811 can provide low specific costs, despite their high active material cost. In conclusion, the cost of an active material may not be effective on the overall cost of a battery for high-performance applications.

4.2 Recommendations for Future Work

For the next studies on LIB production cost optimization and obtaining the optimized design for a LIB a few recommendations are listed below:

- Process-based cost model can be updated according to different locations. The best design with the minimum cost can be identified for each country considering their land, energy, and labor costs and access to the materials. Moreover, for some process steps, the assumptions of equipment costs and processing rates are taken from an older version of BatPaC due to the lack of information in the latest BatPac. Interviewing the OEMs and experts for obtaining the most recent trends in battery manufacturing can be done in the future to develop a more accurate cost model.
- The battery cost model can be coupled with a degradation and lifetime estimation model for investigating the degradation effects on the production cost and design of a lithium-ion battery. Predicting the life of the produced bat-

tery can help the manufacturer to analyze the economic aspects of recalling the produced batteries for the scrap and recycling process.

- The cost-effectiveness of state-of-art cathode and anode active materials such as Nickel-Manganese-Cobalt (NMC955) or silicone-doped anodes can be investigated with the tool developed in this study by implementing the new electrochemical properties and processing methods of these new materials in our model.

- Vehicle requirements can be customized even further. An advanced vehicle simulation can be applied to collect precise performance requirements such as power and energy for the vehicle that will be equipped with the designed LIB. The thermal management and battery management systems used in this research were taken from BatPaC's default options. The model can be improved by suggesting new thermal management and battery management systems. These components' size, location, and design can be optimized along with the battery. Each design suggestion's effect on the performance and cost of the battery can be explored.

- The fast-charging equations used in this study were adopted from BatPaC 5.0. They have developed these equations by correlation of a data set taken from charging tests of a single cell type with specific cathode chemistry. An improved fast-charging model can be implemented for new cells.

- Other optimization algorithms can be explored to find better possible solutions.

Bibliography

[1] E. S. Islam, S. Ahmed, and A. Rousseau, "Future battery material demand analysis based on us department of energy r&d targets," *World Electric Vehicle Journal*, vol. 12, no. 3, p. 90, 2021.

[2] A. Sakti, J. J. Michalek, E. R. Fuchs, and J. F. Whitacre, "A techno-economic analysis and optimization of li-ion batteries for light-duty passenger vehicle electrification," *Journal of Power Sources*, vol. 273, pp. 966–980, 2015.

[3] K. W. Knehr, J. J. Kubal, P. A. Nelson, and S. Ahmed, "Battery performance and cost modeling for electric-drive vehicles: A manual for batpac v5. 0," tech. rep., Argonne National Lab.(ANL), Argonne, IL (United States), 2022.

[4] IEA, "Global ev outlook 2023: Catching up with climate ambitions," tech. rep., International Energy Agency (IEA), 2023.

[5] J. A. Sanguesa, V. Torres-Sanz, P. Garrido, F. J. Martinez, and J. M. Marquez-Barja, "A review on electric vehicles: Technologies and challenges," *Smart Cities*, vol. 4, no. 1, pp. 372–404, 2021.

[6] D. Linden, "Handbook of batteries," in *Fuel and energy abstracts*, vol. 4, p. 265, 1995.

[7] P. A. Nelson, S. Ahmed, K. G. Gallagher, and D. W. Dees, "Cost savings for manufacturing lithium batteries in a flexible plant," *Journal of Power Sources*, vol. 283, pp. 506–516, 2015.

[8] V. Foundation, "The battery report 2022," tech. rep., Volta Foundation, 2023.

[9] C. McKerracher, "Rising battery prices threaten to derail the arrival of affordable evs." Available at https://www.bloomberg.com/news/articles/2022-12-06/rising-battery-prices-threaten-to-derail-the-arrival-of-affordable-evs (2023/07/01).

[10] F. Duffner, M. Wentker, M. Greenwood, and J. Leker, "Battery cost modeling: A review and directions for future research," *Renewable and Sustainable Energy Reviews*, vol. 127, p. 109872, 2020.

[11] C. Xu, Q. Dai, L. Gaines, M. Hu, A. Tukker, and B. Steubing, "Future material demand for automotive lithium-based batteries," *Communications Materials*, vol. 1, no. 1, p. 99, 2020.

[12] M. Armand, P. Axmann, D. Bresser, M. Copley, K. Edström, C. Ekberg, D. Guyomard, B. Lestriez, P. Novák, M. Petranikova, *et al.*, "Lithium-ion batteries–current state of the art and anticipated developments," *Journal of Power Sources*, vol. 479, p. 228708, 2020.

[13] J. Li, Z. Du, R. E. Ruther, S. J. An, L. A. David, K. Hays, M. Wood, N. D. Phillip, Y. Sheng, C. Mao, *et al.*, "Toward low-cost, high-energy density, and high-power density lithium-ion batteries," *Jom*, vol. 69, pp. 1484–1496, 2017.

[14] D. L. Wood III, J. Li, and C. Daniel, "Prospects for reducing the processing cost of lithium ion batteries," *Journal of Power Sources*, vol. 275, pp. 234–242, 2015.

[15] R. E. Ciez and J. Whitacre, "Comparison between cylindrical and prismatic lithium-ion cell costs using a process based cost model," *Journal of Power Sources*, vol. 340, pp. 273–281, 2017.

[16] A. Sakti, I. M. Azevedo, E. R. Fuchs, J. J. Michalek, K. G. Gallagher, and J. F. Whitacre, "Consistency and robustness of forecasting for emerging technologies: The case of li-ion batteries for electric vehicles," *Energy Policy*, vol. 106, pp. 415–426, 2017.

[17] F. Wang, Y. Deng, and C. Yuan, "Design and cost modeling of high capacity lithium ion batteries for electric vehicles through a techno-economic analysis approach," *Procedia Manufacturing*, vol. 49, pp. 24–31, 2020.

[18] N. Xue, W. Du, T. A. Greszler, W. Shyy, and J. R. Martins, "Design of a lithium-ion battery pack for phev using a hybrid optimization method," *Applied Energy*, vol. 115, pp. 591–602, 2014.

[19] A. Epp, R. Wendland, J. Behrendt, R. Gerlach, and D. U. Sauer, "Holistic battery system design optimization for electric vehicles using a multiphysically coupled lithium-ion battery design tool," *Journal of Energy Storage*, vol. 52, p. 104854, 2022.

[20] A. Tomaszewska, Z. Chu, X. Feng, S. O'kane, X. Liu, J. Chen, C. Ji, E. Endler, R. Li, L. Liu, *et al.*, "Lithium-ion battery fast charging: A review," *ETransportation*, vol. 1, p. 100011, 2019.

[21] J. Song, Z. Liu, K. W. Knehr, J. J. Kubal, H.-K. Kim, D. W. Dees, P. A. Nelson, and S. Ahmed, "Pathways towards managing cost and degradation risk of fast charging cells with electrical and thermal controls," *Energy & Environmental Science*, vol. 14, no. 12, pp. 6564–6573, 2021.

[22] T. Yüksel, *Quantification of Temperature Implications and Investigation of Battery Design Options for Electrified Vehicles*. PhD thesis, Carnegie Mellon University Pittsburgh, PA, 2015.

[23] I. Weustink, E. Ten Brinke, A. Streppel, and H. Kals, "A generic framework for cost estimation and cost control in product design," *Journal of Materials Processing Technology*, vol. 103, no. 1, pp. 141–148, 2000.

[24] C. Bloch and R. Ranganthan, "Process based cost modeling," in *[1991 Proceedings] Eleventh IEEE/CHMT International Electronics Manufacturing Technology Symposium*, pp. 406–412, IEEE, 1991.

[25] P. A. Nelson, S. Ahmed, K. G. Gallagher, and D. W. Dees, "Modeling the performance and cost of lithium-ion batteries for electric-drive vehicles," tech. rep., Argonne National Lab.(ANL), Argonne, IL (United States), 2019.

[26] G. Zubi, R. Dufo-López, M. Carvalho, and G. Pasaoglu, "The lithium-ion battery: State of the art and future perspectives," *Renewable and Sustainable Energy Reviews*, vol. 89, pp. 292–308, 2018.

[27] "Byd's revolutionary blade battery: all you need to know." Available at https://www.byd.com/eu/blog/BYDs-revolutionary-Blade-Battery-all-you-need-to-know.html (2023/07/12).

[28] W. B. Hawley and J. Li, "Electrode manufacturing for lithium-ion batteries—analysis of current and next generation processing," *Journal of Energy Storage*, vol. 25, p. 100862, 2019.

[29] "Samsung sdi automotive battery products." Available at https://www.samsungsdi.com/automotive-battery/products/prismatic-lithium-ion-battery-cell.html (2023/07/14).

[30] J.-Y. Kim, B.-S. Lee, D.-H. Kwon, D.-W. Lee, and J.-K. Kim, "Low voltage charging technique for electric vehicles with 800 v battery," *IEEE Transactions on Industrial Electronics*, vol. 69, no. 8, pp. 7890–7896, 2021.

[31] C. Jung, "Power up with 800-v systems: The benefits of upgrading voltage power for battery-electric passenger vehicles," *IEEE Electrification Magazine*, vol. 5, no. 1, pp. 53–58, 2017.

[32] P. Makeen, H. A. Ghali, and S. Memon, "A review of various fast charging power and thermal protocols for electric vehicles represented by lithium-ion battery systems," *Future Transportation*, vol. 2, no. 1, p. 15, 2022.

Appendix A

The optimized design, costs and battery performance parameters are given in tables A.1 and A.2 for the relaxed boundaries case.

Table A.1: Performance parameters and dimensions of optimized designs for relaxed boundaries case

	Pack energy (kWh)	Pack power (kW)	Pack voltage (V)	Cell capacity (Ah)	Pack length (mm)	Pack width (mm)
NMC811						
PHEV30	8.25	45.02	103.1	76.61	239.25	546.9
PHEV60	16.93	49.35	135.12	120.0	342.8	580.15
BEV200	60.59	165.2	241.8	120.0	959.07	597.6
BEV300	92.2	251.9	245.3	120.0	1417.7	597.98
NMC622						
PHEV30	8.04	44.77	100.52	77.51	257.2	526.34
PHEV60	16.89	49.2	136.42	120.0	363.05	573.03
BEV200	59.57	170.55	240.5	120.0	955.12	607.23
BEV300	92.03	264.51	247.7	120.0	1427.8	608.36
LFP						
PHEV30	8.13	44.28	101.74	78.96	315	538.7
PHEV60	16.75	62.85	137.84	120.0	427.47	608.64
BEV200	59.05	223.0	242.86	120.0	1310.5	608.64
BEV300	92.16	310.23	252.71	120.0	1473.8	698.75
NCA						
PHEV30	8.19	44.61	102.4	76.38	239.57	548.77
PHEV60	16.86	48.97	134.21	120.0	343.57	582.63
BEV200	60.36	162.78	240.17	119.99	969.38	597.79
BEV300	93.21	254.03	247.24	120.0	1437.7	601.21

Table A.2: Relaxed boundaries case results

	Cathode Thickness (μm)	# of bi-cell layers	Cathode width (mm)	# of series cells per module	# of modules per row	# of rows of modules	# of cells in parallel	Pack cost ($)	Pack specific cost ($/kWh)
NMC 811									
PHEV30	82.3	11	144.8	29	1	1	1	2360.5	286
PHEV60	155.17	8	154.7	38	1	1	1	3250.9	192.0
BEV200	163.86	7	161.0	68	1	1	2	8383.8	138.35
BEV300	163.6	7	161.13	69	1	1	3	11981.4	129.92
NMC 622									
PHEV30	95.0	12	137.3	28	1	1	1	2369.38	294.64
PHEV60	180.0	8	151.98	38	1	1	1	3332.4	197.24
BEV200	176.4	7	164.16	67	1	1	2	8591.8	144.21
BEV300	175.5	7	164.5	69	1	1	3	12460	135.4
LFP									
PHEV30	148.1	12	140.43	31	1	1	1	2384.7	292.98
PHEV60	200	10	163.2	42	1	1	1	3365.2	200.81
BEV200	200	10	163.20	74	1	1	2	8615.5	145.89
BEV300	200	7	195.0	77	1	1	3	12715	137.95
NCA									
PHEV30	83.92	11	145.44	29	1	1	1	2382.5	290.75
PHEV60	158.4	8	155.59	38	1	1	1	3300.7	195.68
BEV200	169.0	7	161.0	68	1	1	2	8570.8	141.97
BEV300	166.56	7	162.2	70	1	1	3	12421	133.25